# Detection and High Resolution Tracking of Vehicles at Hypersonic Velocities

Author:

William Culbreth, Ph.D.
Department of Mechanical Engineering
University of Nevada, Las Vegas

Contents

Figures

Tables

Introduction

An object is supersonic when its speed through the atmosphere is greater than the local speed of sound. The Mach number is defined as the speed of the object divided by the local speed of sound. For Mach numbers greater than 1 (supersonic flow), shock waves develop in the flowfield and near the surface of the object due to the air's compressibility. Traditionally, the lower Mach number limit for the so-called hypersonic speed regime is about Mach 5 (1.7 km/sec). "Low hypersonic" values range between Mach 5 to about Mach 10, while "high hypersonic" values range between approximately Mach 10 to Mach 30 or above. Mach 30 (10 km/s), for example, is close to Space Shuttle reentry velocity. Few objects can travel at hypersonic velocities. The most common object that we see moving at these speeds are meteors entering the Earth's atmosphere. As meteors fall to the Earth's surface, their velocities may reach 30 miles per second (48 km/s),[1] and their corresponding Mach number as they enter the upper layers of the atmosphere will exceed 150. Meteors are preceded by a bow shockwave as they compress the air immediately in their path. Temperatures and pressures increase dramatically across the shockwave to a point where the gases in air ionize and disassociate, leading to the emission of visible light and radio waves. These conditions also lead to rapid heating of the meteor surface causing them to fracture and break up as they enter the atmosphere. Optical and RADAR-based surveillance systems are now used to scan outer space to detect asteroids and other objects with orbits that may lead them to collide with Earth.

A second class of hypersonic objects includes reentry vehicles moving into the Earth's atmosphere from orbit. In the case of a reentry vehicle returning from low-Earth orbit at 100 km altitude, the velocity of the vehicle will reach 8 km/s (about 5 miles per second). The Mach number of this vehicle will exceed 26.5 in the upper atmosphere. As the vehicle moves through the atmosphere, flow-induced drag forces will slow down the vehicle; if the vehicle has sufficient thermal protection, it can survive reentry and be recovered.

A third class of hypersonic vehicles includes the reentry payload used in ICBMs (intercontinental ballistic missiles). The payload in these missiles is launched using a rocket that boosts them above the atmosphere to a suborbital velocity. The payload velocity may exceed 7 km/s as they reenter the atmosphere, equating to M > 23. The coupled high velocity and high kinetic energy of these objects creates an ionized wake and shock wave that can be used to detect their position and to determine their velocity. This information, along with their ballistic trajectory, is used to locate their target and the time to impact.

A fourth class of hypersonic vehicles includes manned and unmanned rockets and aircraft. The North American X-15, for example, exceeded a speed of 7,274 km/hr in 1964, equating to about M = 6.5. This aircraft also exceeded 100 km in altitude on two occasions, qualifying the X-15 as a spacecraft. The SR-71 Blackbird, an air-breathing strategic reconnaissance aircraft, has exceeded Mach 3.2 at 80,000-ft altitude, and its actual maximum speed may have reached into the hypersonic flow regime. Other real and conceptual aircraft capable of reaching hypersonic speeds include the alleged Aurora SR-91 (Mach 4 to 6), the Boeing X-51, an unmanned Mach 6 scramjet, the HTV-2 from the DARPA Falcon project (designed for M=20 flight to low-Earth orbit), the HyperSoar (M = 12), the Russian Leninetz Ayaks, and the Skylon (designed for single-stage-to-orbit flights). Certain rockets are also designed to travel at hypersonic speeds. The Patriot missile, for example, travels at Mach 5, a high speed necessary for it to be able to intercept and destroy other missiles while they are in flight.

1

There are a number of different techniques available to detect hypersonic objects and to determine their position, velocity, and trajectory. These detection methods can be broadly divided into electromagnetic, optical, and acoustic/seismic methods. Each method relies on the properties of the surface of the object to reflect incident radiation or upon the properties of the hot ionized gases caused by the bow shock and entrained into the object's wake. The theory of external fluid flow around objects in subsonic, supersonic, and hypersonic regimes will be reviewed and various detection methods will be compared in this report.

2

Chapter 1: Theory Governing Objects in Flight

Many of the detection technologies for hypersonic aircraft are based on the properties of the air flow around the object. The fluid mechanics affecting supersonic and hypersonic aircraft are well described in textbooks on compressible flow by J.D. Anderson;[2,3] subsonic flow, including the affect of boundary layers, is covered in the textbook by F. M. White.[4]

Hypersonic flow usually refers to the regime where objects are moving faster than Mach 5, but technically refers to the Mach range where pressure, temperature, and density ratios across shock waves reach constant values, and this does happen at about Mach 5. Fluid flow changes dramatically at Mach 1 defined at the point where the velocity of a projectile, V, equals the local speed of sound, a, in the atmosphere:

$$M = \frac{V}{a}$$
(1)

Flow regimes are defined by the following:

- $M < 1$, subsonic flow
- $M = 1$, sonic flow
- $M > 1$, supersonic flow
- $M > 5$, hypersonic flow

The speed of sound varies with temperature and with the type of gases in the atmosphere. A simple equation for the speed of sound includes the ratio of specific heats, γ, the gas constant, R, and the temperature, T:

$$a = \sqrt{\gamma R T}$$
(2)

For air at room temperature, $\gamma = 1.4$, R = 287 J/kg·K, and T = 20° C or 293 K. The subsequent speed of sound is 343 m/s (1,125 ft/s or 767 mph). It is easier for a projectile to exceed the speed of sound at higher elevations since the temperature of the atmosphere is lower, reducing the speed of sound and the subsequent velocity necessary to break the sound barrier.

The viscosity of the fluid flowing around an object induces drag and retards its forward motion. Supersonic flow has some of the viscous characteristics of subsonic flow, but adds in the complication of shock waves. To understand the nature of how a projectile affects the flow of fluid around it, consider the case of a subsonic projectile.

SUBSONIC FLOW AND DRAG

Subsonic flows, such as the flow shown in Figure 1, are heavily influenced by collisions between molecules of air and the surface of the projectile. The equations for this interaction were first developed by Sir Isaac Newton in the seventeenth century, where he determined that fluids have a property called "viscosity" that is the cause of drag on projectiles. The key parameter that affects subsonic fluid flow is the ratio of viscous forces to inertial forces, where inertial forces are associated with the tendency for a moving fluid to keep moving in the same direction. The ratio of these two forces is defined as the Reynolds Number, Re.

3

$$\mathrm{Re} = \frac{viscous\ forces}{inertial\ forces} = \frac{V\ D}{v} \qquad (3)$$

In this expression, V is the velocity of the projectile, D is its effective diameter, and v is the kinematic viscosity of the fluid. As flow passes over the projectile in Figure 1, viscous forces are especially strong near the surface where the velocity changes from zero at the surface of the projectile to the free stream velocity.
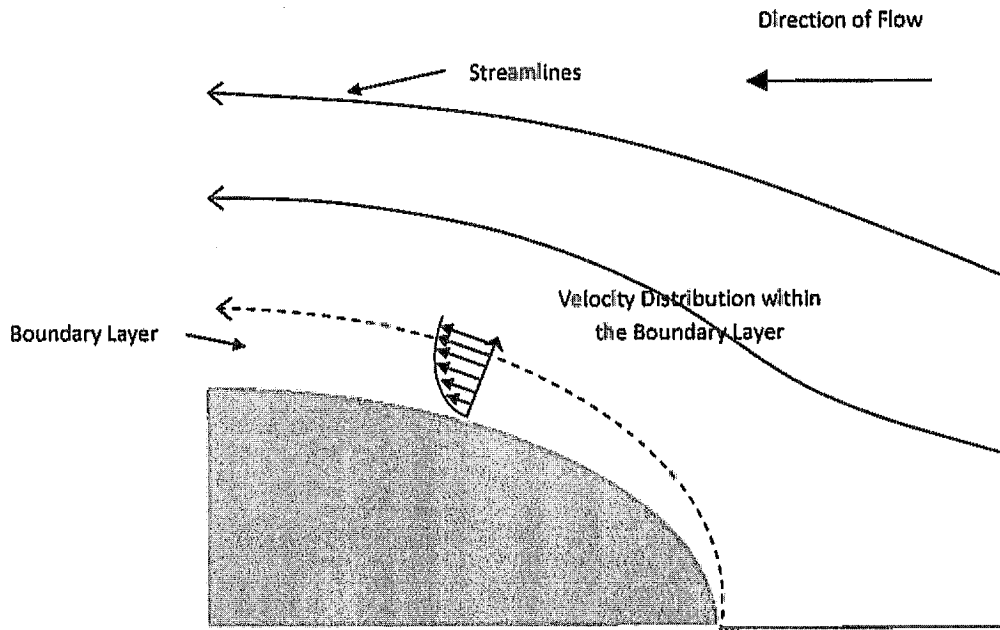
Figure 1. Boundary Layer Development in Subsonic Flow About a Projectile.

The region where this transition in velocity occurs is called a "boundary layer," which grows in thickness as flow moves along the surface from the nose to the rear of the projectile. The boundary layer forms around the surface of the projectile and "separates" from the surface at the back end of the projectile. Pockets of fluid spill off of the back end of the projectile and form rotating pockets of fluid called Strouhal eddies or vortices. These eddies "shed" from the surface at a rate that is strongly dependent upon the Reynolds number in the flow. Figure 2 demonstrates that these eddies form a "wake" downstream of the projectile that can extend far into the fluid.

4

Boundary Layers

Strouhal Eddies or Vortices

Streamlines

Turbulent Wake

Projectile

Direction of Flow
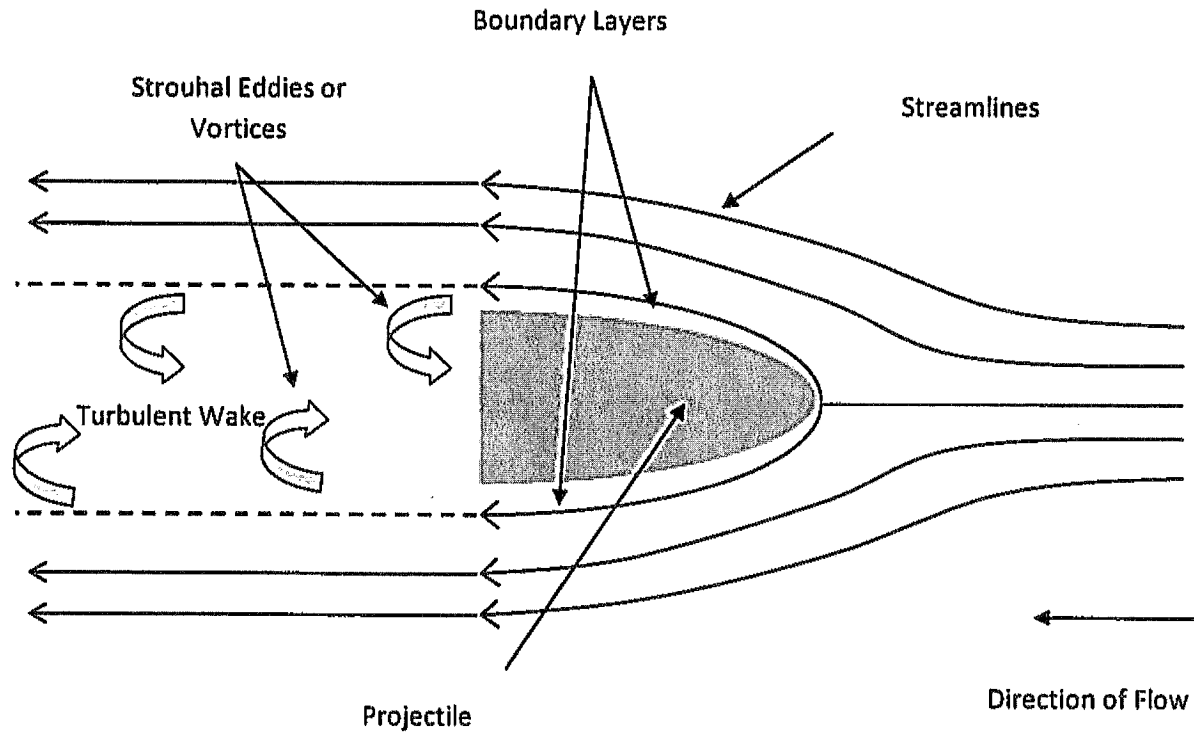
Figure 2. Subsonic Flow Past a Projectile.

Visible examples of a "wake" are the contrails observed in the upper atmosphere when water vapor in the exhaust of jet aircraft freezes into ice crystals, highlighting the wake generated by the aircraft and its engines. In still air, the wake can be visible for many miles behind the aircraft.

The wake rapidly becomes turbulent as it extends downstream. The Strouhal eddies are detectable and have a shedding frequency that is expressed in terms of the Strouhal number, $St = f\,D/V$, where f is the Strouhal shedding frequency (hz), D is the diameter (m) of the projectile, and V is its velocity (m/s) through the air. The Strouhal number is a function of Reynolds number, as shown in Figure 3. By measuring the Strouhal frequency, the velocity of the projectile can be determined with moderate accuracy.

At low speeds, and corresponding low Reynolds numbers, the flow is "laminar" where streamlines move in smooth "laminae" or layers over projectiles. At high Reynolds numbers, the fluid flow becomes unstable and forms a widely distributed set of small eddies defined as "turbulence." In turbulent flow, rapid mixing of the flow in the wake, even in the boundary layers, will occur.

5
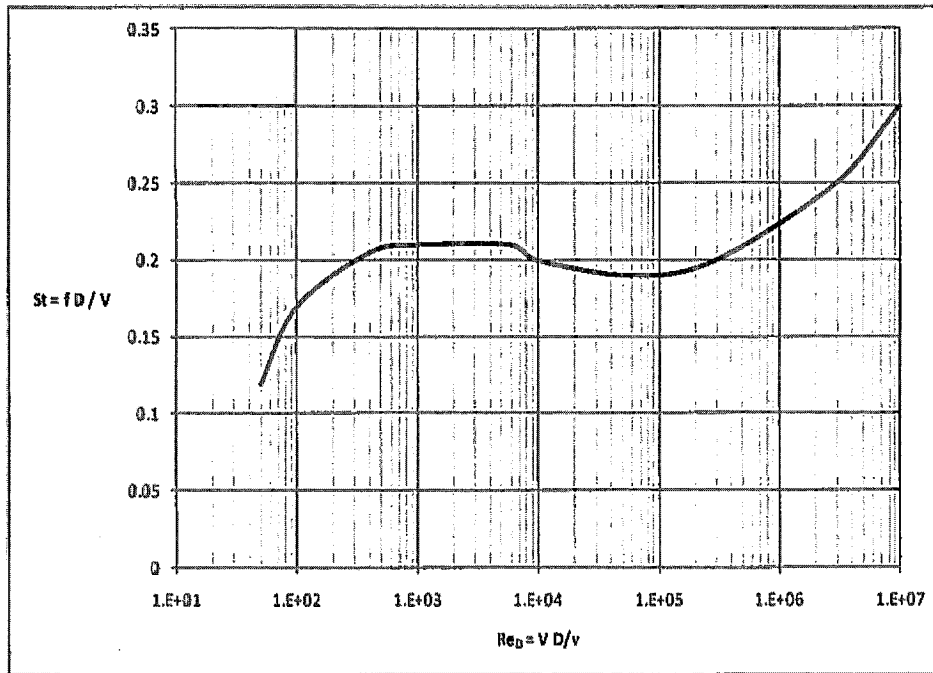
Figure 3. Strouhal Frequency as a Function of Reynolds Number for Flow Over a Circular Cylinder.

The high velocities present in the wake generate low pressures on the downstream side of the projectile that pull the projectile backwards into the wake. This is defined as "wake" or "form" drag and is a predominant cause of drag forces on aircraft or on any object moving through the atmosphere. The viscous forces that create the boundary layers on the surface of a projectile also contribute a small amount of drag, usually referred to as "skin friction." Boundary layers and wakes also affect supersonic flow, but the effect of shock waves tends to be the predominant mechanism affecting flow around supersonic projectiles. Total drag force, F_D, exerted on projectiles or aircraft is usually summarized by this equation:

$$F_D = \frac{1}{2} \rho \, A_f \, C_D \, V^2 \tag{4}$$

The drag force is dependent upon the density of the air, ρ, the frontal area of the aircraft, A_f, the aircraft velocity, V, and the drag coefficient, C_D. The drag coefficient is a function of the geometry of the aircraft and the two "dimensionless" groups, Mach number, M, and Reynolds number, Re_D, that relate inertial, viscous, and elastic forces in the flow:

$$C_D = f(\mathrm{Re}_D, M, geometry) \tag{5}$$

Drag coefficients for various types of aircraft and projectiles are obtained from theory, from computational fluid mechanics, or, most commonly, from experiments in wind tunnels. These coefficients are usually presented in tables or in graphical form.[5, 6, 7]

SUPERSONIC FLOW

Air is predominantly made up of molecules of nitrogen (78%) and oxygen (21%). At room temperature, air behaves as an ideal gas where the density, ρ, the pressure, p, and the temperature, T, are related through a gas constant, R, which is a property of the air. The ideal gas law gives the relationship between these values. The gas constant for air is $R = 287$ J/kg·K.

6

$$p = \rho R T \tag{6}$$

It is possible to statistically model the motion of the molecules of oxygen and nitrogen in air, and their kinetic energy, KE, can be determined based on the mass, m, of each molecule and the temperature of the gas.

$$KE = \frac{1}{2} m V^2 = \frac{3}{2} k T \tag{7}$$

In this equation, k is the Boltzmann constant (1.3807×10^{-23} J/K). We can calculate the velocity of air molecules based on the temperature of the air.

$$V = \sqrt{\frac{3 k T}{m}} \tag{8}$$

Or, for the average velocity of a molecule:

$$\overline{V} = \sqrt{\frac{8 R T}{\pi}} \tag{9}$$

For air near sea level (p = 101,320 Pa, T = 293 K) the average velocity of molecules in air is 463 m/s or 1,035 MPH. This value is just a little higher than the speed of sound in air (343 m/s or 767 MPH) as computed earlier. These molecules only travel a short distance before they collide with each other. This distance is defined as the "mean free path" given by the symbol λ.

$$\lambda = \frac{1}{\sqrt{2} \, \pi \, d^2 \, \rho} \tag{10}$$

In this expression, d is the diameter of a molecule, which is approximately 0.3 nanometers. For air at 20° C and 101,325 Pa, the mean free path (λ) is approximately 100 nanometers or about 333 molecular diameters.

When the supersonic projectile in Figure 4 moves through the air, molecules of nitrogen and oxygen in the air bounce off the vehicle's surface and collide with other molecules of air a short distance away. At the speed of sound, these molecules are not moving fast enough to get out of the way and a large number of molecules pile up along a straight line that emanates from the nose or leading edge of the projectile as a "shock wave."

Supersonic flow in the atmosphere labeled as region 1 passes through the shock and moves parallel to the surface of the body. The flow "expands" through a Prandtl-Meyer expansion fan at the end of the airfoil and speeds back up to its original Mach number. Flow in the boundary layer separates from the end of the airfoil and forms a highly turbulent wake downstream of the airfoil. The wake is also composed of Strouhal eddies that can subsist in the air long after the airfoil has passed by. The flow density, pressure, and temperature increases dramatically across the bow shockwave and returns to the original Mach number downstream of the airfoil.

For a blunt-nosed object, as shown in Figure 5, the magnitude of the impact that the shockwave has on the flow is easier to explain. For a blunt object, the shock detaches from the surface of the object into the freestream in front of the object. Since the original flow moving at M_1 is traveling at 90° with respect to the shock near the nose of the object, the shock in this region is referred to as a "normal" shock. The properties across a normal shock

are described by the Rankine-Hugoniot equations, which yield the ratio of certain thermodynamic properties.
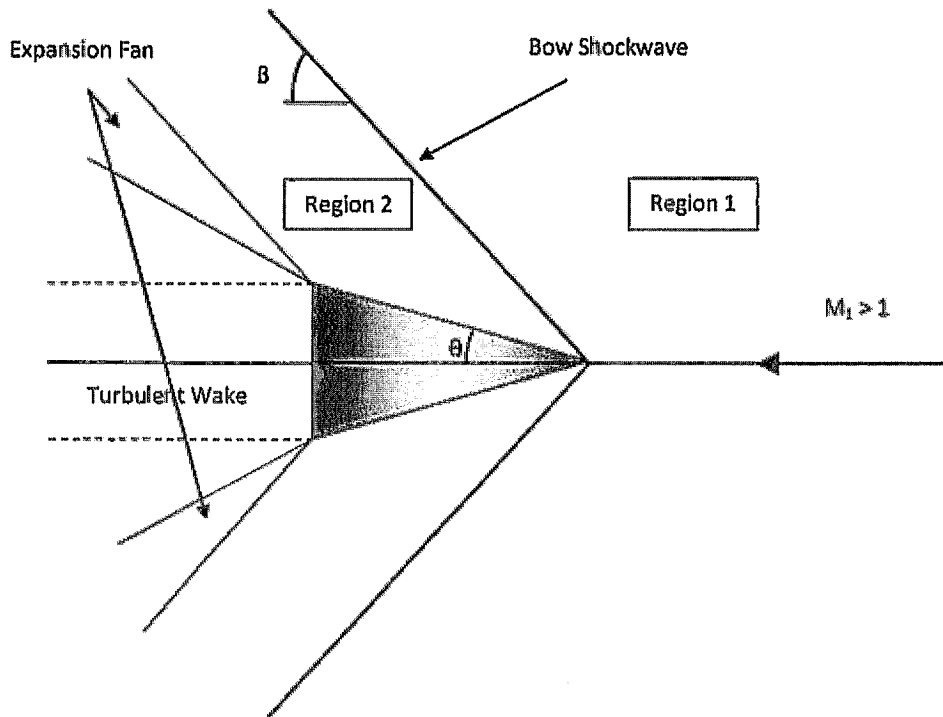

Figure 4. Supersonic Flow Past a Wedge-Shaped Body.
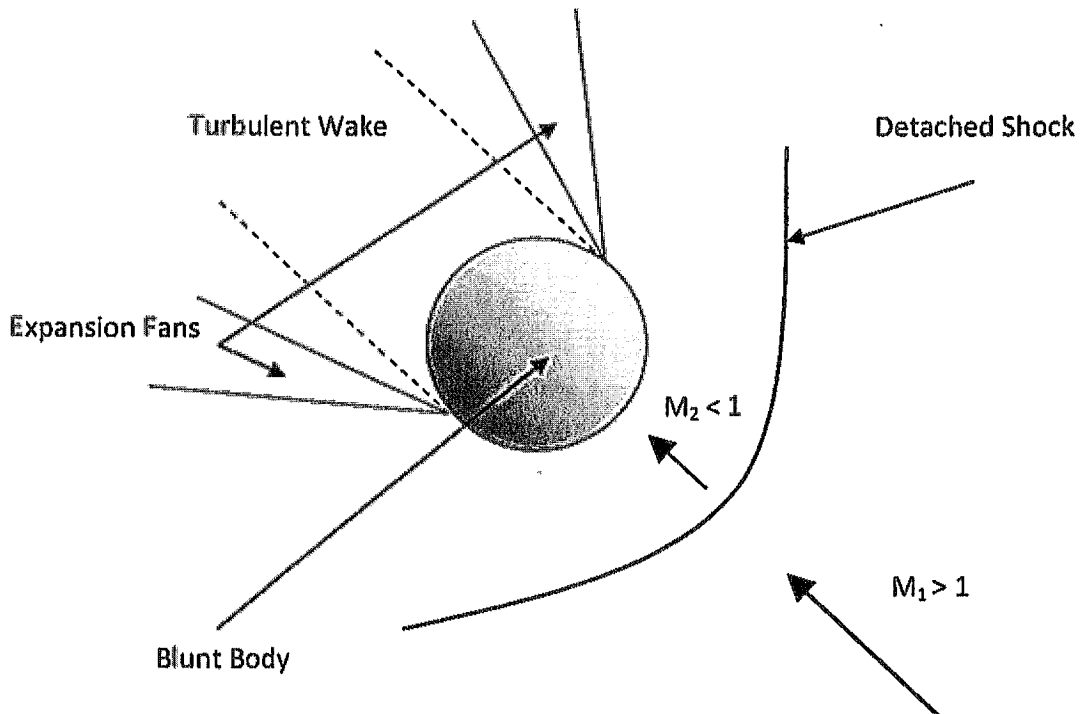
Figure 5. Supersonic Flow Past a Blunt Body (Spheroid).

These equations can be expressed in a form where the ratio of density, temperature, and pressure across the normal shock are a function of the upstream Mach number, M_1.

$$\frac{M_2}{M_1} = \sqrt{\frac{1 + \frac{\gamma - 1}{2} M_1^2}{\gamma M_1^2 - \frac{\gamma - 1}{2}}} \tag{11}$$

$$\frac{T_2}{T_1} = \left[1 + \frac{2\gamma}{\gamma + 1}\left(M_1^2 - 1\right)\right]\left[\frac{2 + (\gamma - 1) M_1^2}{(\gamma + 1) M_1^2}\right] \tag{12}$$

$$\frac{p_2}{p_1} = 1 + \frac{2\gamma}{\gamma + 1}\left(M_1^2 - 1\right) \tag{13}$$

$$\frac{\rho_2}{\rho_1} = \frac{(\gamma + 1) M_1^2}{2 + (\gamma - 1) M_1^2} \tag{14}$$

As an example, if the object shown in figure 4 is traveling at Mach 3 through air at sea level, the pressure in the region between the nose of the object and the shock changes as shown in the following table:

Table 1: Normal Shock Values for Mach 3 Flow

Freestream Values	Ratio of Properties Across the Normal Shock	Values Downstream of the Normal Shock
$M_1 = 3$	$M_2/M_1 = 0.158$	$M_2 = 0.475$
$p_1 = 101,325$ Pa	$p_2/p_1 = 10.333$	$p_2 = 1,047,000$ Pa
$T_1 = 293$ K	$T_2/T_1 = 2.679$	$T_2 = 785.0$ K
$= (20°C)$		$= (512°C)$
$\rho_1 = 1.293$ kg/m³	$\rho_2/\rho_1 = 3.857$	$\rho_2 = 4.976$ kg/m³

For a normal shock, the Mach number on the downstream side of the shock is always subsonic, and in this example, the Mach number abruptly drops from $M_1 = 3$ to $M_2 = 0.475$. The temperature always increases across a shock, and for a Mach 3 flow, the temperature rises from room temperature at 20° C up to 512° C. It is apparent that, for supersonic aircraft traveling at this speed, the fuselage and wings will need to be made of materials that can withstand the high temperatures and the dramatic pressure increase of 10.333. Shocks are always accompanied by significant increases in pressure, temperature, and density in the flow across the shock.

Flow about an Ogive or wedge-shaped airfoil as shown in Figure 4 can be analyzed in a similar fashion; however, the wall deflection angle, θ, will affect the flow and the formation of the oblique shock wave that surrounds the airfoil.

9

Chapter 2: Hypersonic Compressible Flow Theory

Hypersonic flow is typically assumed to apply to objects traveling at M > 5. Figure 6 shows that, for Mach numbers above 5, the ratio of Mach numbers across the shock approaches a constant value of 0.378, although temperature and pressure ratios continue to increase. In hypersonic flow, the bow shock, or Mach angle, β, approaches the half-angle, θ, of slender airfoils and the drag coefficient reaches a constant value that does not change with Mach number. The drag coefficient actually becomes a simple function of the half-angle of the airfoil, and the boundary layer is squeezed between the shockwave and the airfoil surface.
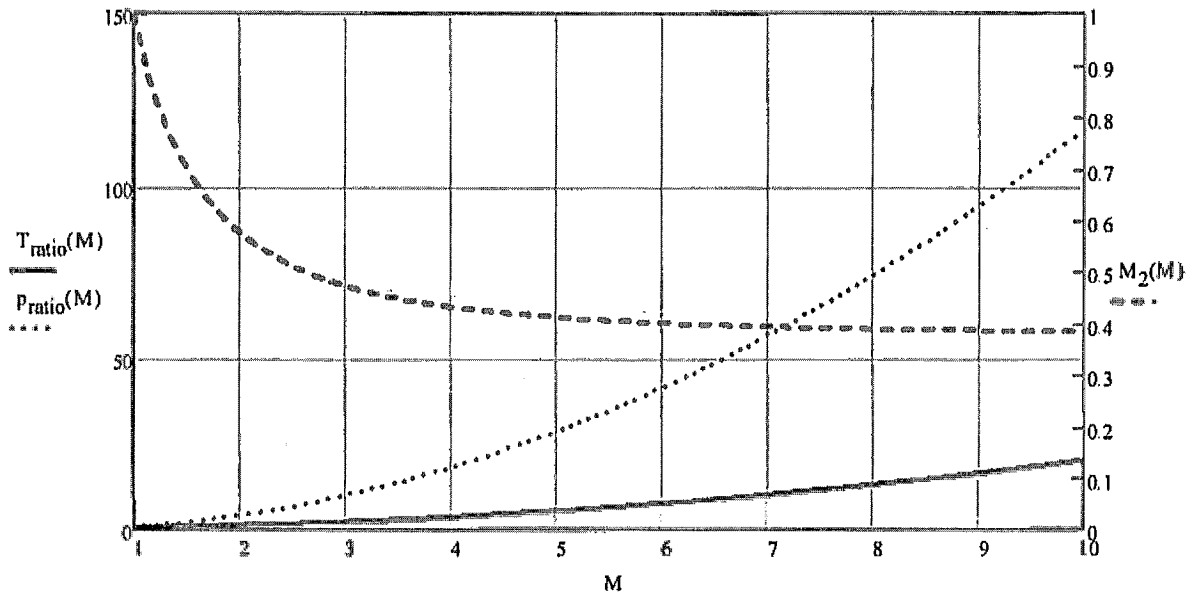
Figure 6. Ratios of Mach Number, Temperature, and Pressure Across a Normal Shock

In hypersonic flow, the Rankine-Hugoniot equations, which are based on the perfect gas law ($p = \rho RT$), fail to predict the real behavior of air at extremely high temperatures. Equation 12, for example, predicts a temperature of 29,787° C in the air near the surface of a blunt object traveling at the reentry Mach number of 26.5, while the actual temperature only reaches 7,600° C. The reason for this discrepancy is due to ionization of molecules of air as electrons are stripped away by the high temperatures that exist across the shock. Some energy is used to produce this ionization, and above temperatures of 550° C, equation 15 does not accurately predict air temperatures due to shocks. Ionization is responsible for the glowing wake that follows reentry vehicles and meteors as electrons rush to recombine with ions releasing x-rays and visible light. The ionization also interferes with radio transmissions, but provides a convenient way to identify hypersonic objects due to the emitted light. A "rule of thumb" is that the peak shock layer temperature in degrees kelvin is 1,000 times larger than the aircraft speed in km/s. By this standard, a reentry vehicle at 8 km/s (Mach 26.5) would have a maximum shock layer temperature of 8,000 K. At temperatures above 2,000 K, nitrogen and oxygen gas in the form of O_2 and N_2 will disassociate into individual ions, consuming more energy from the flow.

Chapter 3: Detection Technologies

Hypersonic objects passing through the Earth's atmosphere leave traces that can be observed using a number of detection methods. The bow shock introduced by such objects reflects and refracts radio waves, RADAR pulses, and visible light. The ionized air surrounding the object also creates electromagnetic interference that is visible on RADAR and the emitted visible light in the wake is observable in photographs. The shock and turbulent wake also create low frequency sound that can be sensed by ground-based sensors. These detection methods can be characterized as electromagnetic, optical, and acoustic and seismic as shown in Figure 7. Each method will be discussed along with the limitations and advantages for the detection of hypersonic objects passing through the atmosphere.

Electromagnetic
RADAR
Energy Reflection
Doppler RADAR
Radio Reflection Detection
Optical
Sky Cameras and Photographic Methods
Infrared Detection
LIDAR
Chronograph
Acoustic and Seismic
Infrasound
Seismic
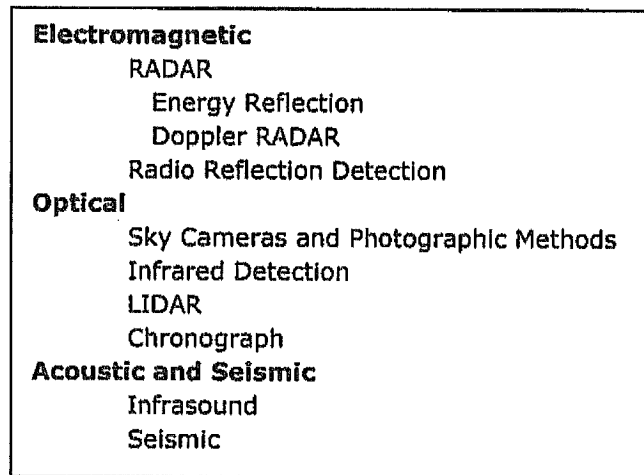
Figure 7. Hypersonic Vehicle Detection Techniques.

One of the fundamental tools for detecting the velocity of high-speed objects is the chronograph. These devices are used to measure the velocity of automobiles using pneumatic tubes, and simple systems using laser diodes or LEDs are used to measure the velocity of bullets. Figure 8 outlines a laser-based chronograph that is commercially available for measuring the velocity of projectiles in two-stage gas guns capable of speeds in a vacuum of 12 km/h, or approximately Mach 36 if the projectile passed through air. As a high-speed object passes through the first laser beam followed rapidly by the second, photodetectors sense the change in intensity of the laser beam and send these signals to a storage oscilloscope or to a counter. The time delay between the two signals, Δt, is used to find the velocity of the object based on the distance between the two photodetectors, L. Digital clocks are capable of accurately measuring time delays to within a fraction of a nanosecond (10^{-9} seconds), so chronographs are capable of very high accuracy in determining the velocity of objects. As noted earlier, their use at gun ranges or in high-speed gas guns requires that the path of the hypersonic object must pass through the laser beams for the chronograph to be effective, which limits their usage for the detection of hypersonic aircraft except at instrumented test ranges.
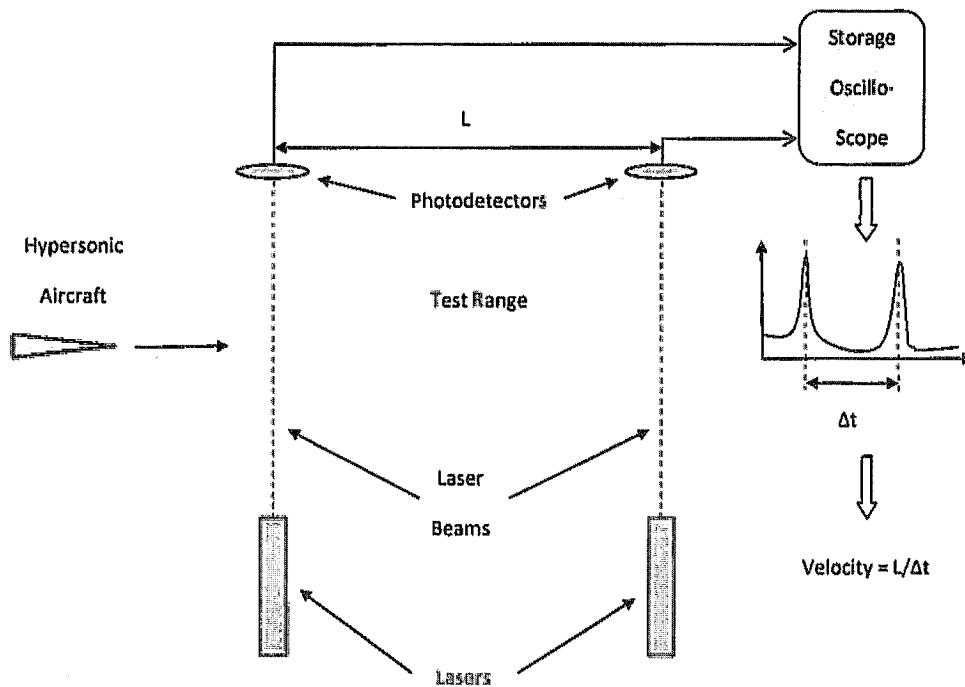
Figure 8. Laser-Based Chronograph.

Currently, the best devices for the detection of hypersonic vehicles are based on the reflection of radio and microwave radiation through RADAR and upon the detection of infrared energy emitted by the ionized gases surrounding high-speed vehicles and in their wake. Optical and RADAR methods are also based on electromagnetic energy, yet make use of different parts of the electromagnetic spectrum as shown in Figure 9. Longer wavelength photons, or quanta of electromagnetic energy, have less energy than short wavelength photons. As a result, detection of short wavelength radiation tends to be more line-of-sight as in infrared or other optical methods. Longer wavelengths, used in RADAR, tend to bend around the Earth and can provide over-the-horizon detection of ICBMs, reentry vehicles, and other hypersonic vehicles.

Electromagnetic Spectrum	
Wavelength	Type of Radiation
1 nm	x-rays
10 nm	
100 nm	Ultraviolet (UV)
1 µm	Visible Light (0.4 to 0.7 µm)
10 µm	Near Infrared
100 µm	Thermal Infrared
1 mm	Far Infrared
10 mm	Microwaves
100 mm	Radar
1 m	Radio Waves
10 m	
100 m	AM Radio

Figure 9. Electromagnetic Spectrum as a Function of Wavelength.

ELECTROMAGNETIC METHODS

RADAR (Reflected Energy)

RADAR, or "radio detection and ranging," has been heavily used since World War II for the detection of aircraft and sea vessels. First patented by Christian Hulsmeyer in 1904, this technique was first demonstrated by Nikola Tesla in 1917; RADAR was exploited in the defense of Britain through the Chain Home RADAR network initiated in the late 1930s.[8] RADAR uses an antenna or a dish to transmit pulses of microwaves or radio waves toward a potential target. Energy reflected from the target is collected by the antenna and the time of flight of the transmitted and reflected signals yields the distance to the target. Early RADAR systems emitted radiation in the high-frequency band (HF) from about 10 to 30 MHz. Modern systems can operate well above 300 GHz.

As a single pulse travels at the speed of light toward a target, the time delay between the generation of the pulse and the time that its echo is received is $2L/c$ where L is the distance to the target and c is the speed of light. For a target located 30 km from the source, the time delay is 200 microseconds, an easily measurable delay. By using microwave radiation emitted from a dish, target distance and bearing can both be measured.

While it was possible to use low-frequency radio waves (~30 MHz) for RADAR systems in the 1940s, the wavelength of these waves (100 meters) made it difficult to resolve small targets, including aircraft. This made it desirable to develop systems that could operate at higher frequencies. UHF energy (300 to 1,000 GHz, 0.3- to 1-meter wavelength) radiation is used for long-range surveillance, including the detection of intercontinental ballistic missiles. Air traffic control uses the L band (1 to 2 GHz, 0.15- to 0.3-meter wavelength). X-band (8 to 12 GHz, 25- to 37-millimeter wavelength) energy is now used for airport RADAR where the range to aircraft is short. Higher frequency radiation is used for imaging systems and for meteorological data acquisition.

13

RADAR systems are widely used for aircraft surveillance and can detect the distance to objects and the position of an object (through triangulation); with Doppler RADAR, the velocity can be directly measured. RADAR does have limitations. While low-frequency RADAR systems are capable of following the curvature of the earth, the long wavelength of this energy makes it difficult to resolve small objects. Higher frequency RADAR tends to be more "line of sight." Since it depends upon reflected energy, several problems are highlighted by the RADAR Equation:

$$P_{received} = \frac{P_{transmitted} \, G \, A \, \sigma \, F^4}{(4\,\pi)^2 \, R_t^2 \, R_r^2} \tag{15}$$

In this equation, $P_{transmitted}$ represents the transmitted power, $P_{received}$ the received power, G the transmitting antenna gain, A the aperture area of the receiving antenna, σ the RADAR cross section, F the pattern propagation factor, and R_t and R_r are the distance from the transmitter to the target and the target to the receiver, respectively. If the RADAR transmitter and receiver are in the same unit, the power returned as a reflection from a target decreases as R^4. This means that energy received in reflected energy decreases by 94% every time the distance to the target is doubled.

RADAR depends upon the reflection of electromagnetic waves off of a target's surface, thereby making objects with a small RADAR cross section difficult to detect (e.g., stealth aircraft). Atmospheric phenomenon, including inversions and turbulence, can lead to interference with RADAR reflections. Even with these limitations, RADAR is widely used to monitor high-speed aircraft, meteors, and man-made objects reentering the atmosphere from Earth orbit.
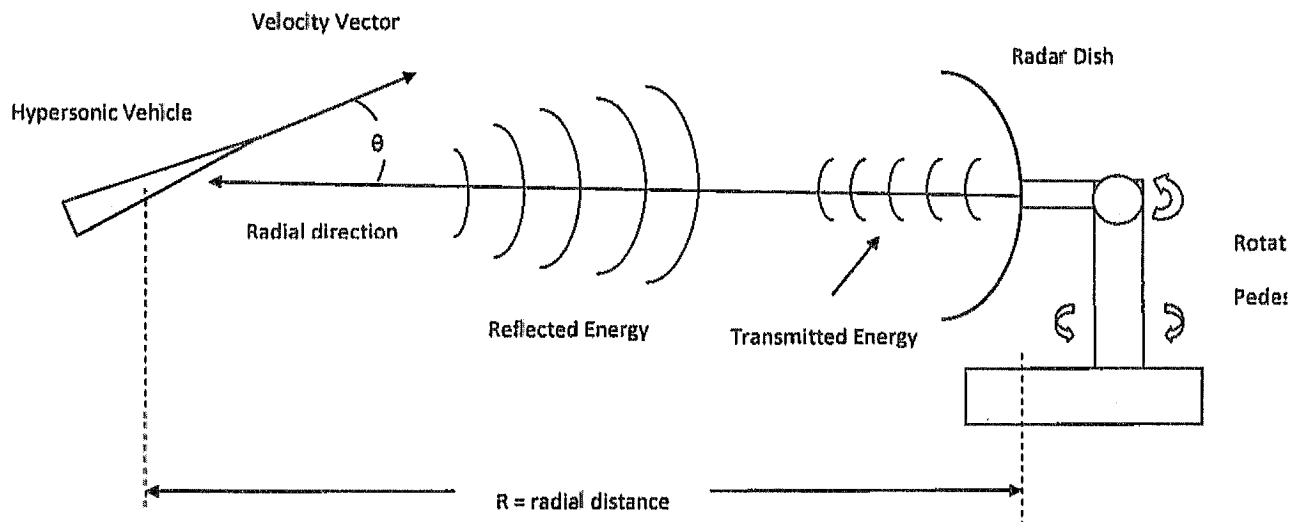
Figure 10. Schematic of a RADAR System.

Doppler RADAR

Doppler RADAR systems yield velocity data for a target. Pulsed RADAR systems send out a short burst of high-frequency radiation that is reflected from a target. The RADAR unit processes the delay time between the transmitted pulse and the received echo to determine the range or distance to the target. The energy reflected from the target is, however,

14

Doppler-shifted from its original frequency due to its velocity toward or away from the RADAR transmitter.[9] The frequency shift, Δf, is given by the following equation:

$$\Delta f = f_{reflected} - f_{transmitted} = \frac{2V}{c-V} f_{transmitted} \approx \frac{2V f_{trasnmitted}}{c} \tag{16}$$

In this equation, c is the speed of light, and V is the target speed in the direction toward or away from the RADAR transmitter. The frequency shift is typically small since $V \ll c$, but the shift is easily observable due to "beating" between the transmitted and reflected signals. The development of fast Fourier transforms (FFTs) greatly increased the rate that Doppler reflections could be processed to compute target velocity. By triangulating between two RADAR transmitters, the position of a target can be determined along with its velocity and direction of travel. Doppler RADAR systems are used for monitoring high-speed aircraft, turbulence and shear in meteorology, and even in hand-held police RADAR guns.

RADAR technology has been used for the detection of missiles, reentry vehicles, and space objects near the Earth since the 1960s. On 9 September 1961, for example, a Naval Research Laboratory RADAR installation at the Chesapeake Bay Annex was used to detect a Mercury/Atlas flight during its launch phase.[10] The RADAR system sensed the range to the rocket, its rate of climb, and the range of its exhaust plume. This RADAR system worked "over the horizon" and demonstrated that a RADAR system could be used to identify targets and compute their trajectory.

A wide range of RADAR systems are now available to monitor the Earth and space for high-speed objects in the atmosphere.[11] Cobra Dane and Cobra Judy, L-band phased-array RADAR systems located on land (Alaska) and on ships (X- and S-band), are used for the detection of reentry vehicles above 35 km. RADAR systems in Florida and Massachusetts are capable of monitoring objects in space at a distance of 5,000 km to yield data on their size and shape. Ballistic missile early warning systems still operate in Alaska, Great Britain, and in Greenland to detect and track missile launches. On Kwajalein Atoll in the Pacific Ocean, *Altar* tracks reentry vehicles at distances of up to 2,500 km with high resolution using a 100-kW, millimeter-wave RADAR system. TRADEX, a multitarget tracking system using L- and S-band RADAR was developed in 1963 to track missile signatures at a distance of up to 1,400 km. The venerable RC-137 (converted Boeing 707) can also be deployed with onboard RADAR and optical systems that can track missile launches and reentry vehicles.

Radio Reflection Detection

This method can be used to detect meteors or any other object entering the Earth's atmosphere during the day or night. The principle of this method is based on passive electromagnetic energy emitted from the Earth's surface in the form of radio or television signals. If these signals are relatively high frequency, the signal is line of sight and cannot normally be received over the horizon. A radio or television located over the horizon and tuned into the signal frequency will only detect static or hiss. When a meteor or other object enters the Earth's atmosphere, its bow shock and turbulent wake containing ionized air reflects radio signals causing an over-the-horizon receiver to hear pings and whistles that change pitch as the meteor passes by and breaks up in the atmosphere.[12] It is possible to receive reflections off of the surface of the hypersonic meteor in addition to the wake and the shock. Sound files from the Aurigid Meteor Shower caused by radio echoes are available[13] with data obtained from a directional antenna at 61 MHz and 217 MHz. The data demonstrates that it is possible to differentiate reflections from the bow shock and the

ionized wake. This technique for detecting hypersonic meteors is not fully developed and appears to be employed only by hobbyists.

Since a receiver can be tuned to a specific over-the-horizon transmitter, it may be possible to develop a network of radio receivers to provide information on high-speed objects in the atmosphere. Multiple stations would allow triangulation of the object to determine velocity and position as a function of time, i.e., tracking and path prediction. The sound files also contain information that could provide information on the hypersonic object. Detection of the shock provides information on the position of the object while the transient "whistles" reflected from the ionized wake may provide information on the Strouhal eddy frequency that could directly infer the object's velocity. This detection technology should be further developed.
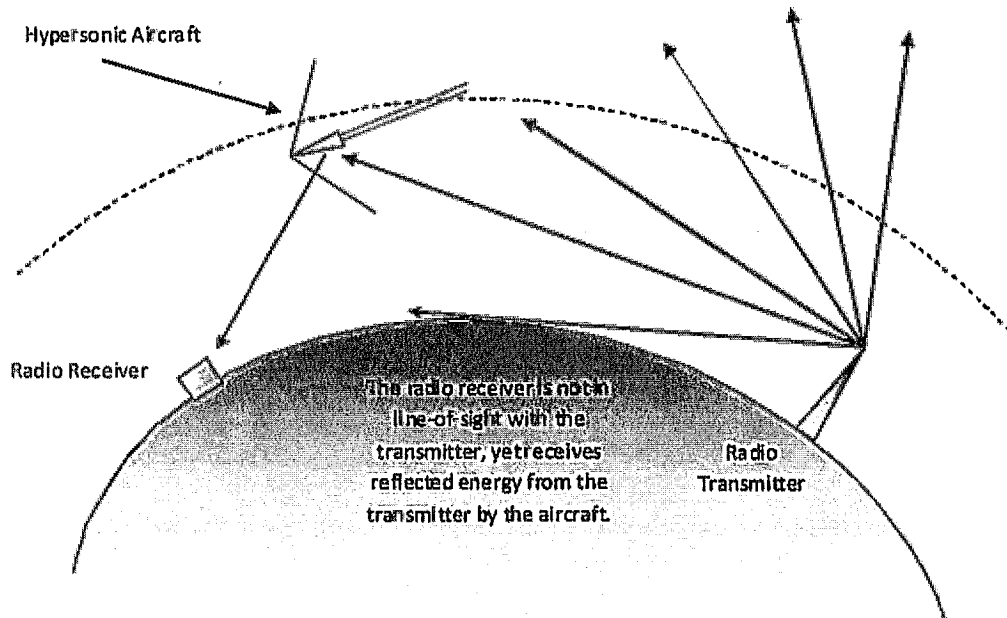
Figure 11. Radio Reflection Detector.

OPTICAL METHODS

Sky Cameras and Photographic Methods

A classic example of a hypersonic object passing through the Earth's atmosphere is a meteor. Meteorite hunters and astrophysicists have worked to develop methods to detect these objects as they fall to the Earth. Motion-detection video systems provide information on location and direction of meteors passing through the atmosphere by detecting their visible wake. The El Paso All Sky Camera project[14] is one example and even provides live streaming video of meteoric events.

Photographs of objects in orbit with diameters ranging from 0.1 meter to several meters have been used to determine their expected trajectory as meteors as they entered and fell through the Earth's atmosphere.[15] This technique was first used to monitor the Pribram meteorite simultaneously by several observatories in 1959. This technique was even used to locate a 1.75-kg enstatite chondrite meteorite called Neuschwanstein reported in 2003. The

16

European Fireball Network[16] uses cameras at several stations separated by distances of about 100 km and covering an area of about 1,000,000 km². Fisheye lenses allow each station to observe the sky every night to monitor meteors and other nebular objects. The network is operated by the German Aerospace Center (DLR) and the Institute of Planetary Research in Prague.[17] Other networks include the Meteorite Observation and Recovery Project (MORP) in Canada and the Prairie Network in the United States; all have been in operation since the 1960s and 70s.

Another recent meteorite recovery was made when asteroid 2008 TC3 entered the Earth's atmosphere on 7 October 2008 over Sudan.[18] The meteor's path left a wake that was visible through dawn. A total of 280 fragments weighing 11 pounds were collected in the Sudanese desert. The photographic evidence of this hypersonic reentry was interesting. The 4.2-meter William Herschel Telescope in the Canary Islands optically recorded the spectrum of this asteroid 2 hours before it burned up in the Earth's atmosphere. This information can be used to identify the chemical makeup of the surface of the object or of the vaporized products in its wake. A sequence of photographs taken at 4-second intervals over a period of about 50 seconds provided information on its velocity as it reentered the atmosphere and its brightness as a function of time.

Although these photographic methods have been applied to meteors, data from the European Fireball Network and similar camera systems can be used to monitor the flight of hypersonic aircraft that produce a visible wake through the ionization of air. The photographic methods described here are limited to nighttime use. Multiple stations recording the same event have been used to measure both position and velocity of objects moving at hypersonic velocities through the Earth's atmosphere and the computed trajectories have been used to successfully predict meteorite impact points on at least two occasions.

Optical systems are constantly monitoring the Earth for possible missile launches. Two KH-II satellites are constantly in orbit 250 to 500 km above the Earth's surface with multispectral cameras that resolve objects to within 2 to 3 meters. Big-Bird, at an orbit 160 to 280 km above the Earth, can take video or photographs with a resolution of 250 mm. The photos must be sent back to Earth for processing. Close-Look, operating from 130 to 300 km, has a resolution of 50 to 150 mm. Landsat, with an orbit of 800 km, can transmit multispectral video of the Earth with a resolution of 20 to 30 meters. The space shuttle, the U-2 aircraft, and the SR-71 have all been used to provide high-resolution images of objects from high altitude.

Infrared Detection

Infrared detection of reentry vehicles and ICBMs by satellites has been available since the early 1960s, with the United States leading the effort through detection of possible missile launches from the Soviet Union. In addition to RADAR, infrared detection is one of the best techniques for the detection of hypersonic vehicles.

Theory of Infrared Detection Systems.

All objects emit radiation that is a function of their temperature according to equation 17, the Stefan-Boltzmann Law:[19]

$$q = \varepsilon\, \sigma\, A\, T^4 \tag{17}$$

17

In this equation, q represents the amount of radiant energy emitted in watts, ε is the emissivity (a dimensionless quantity that gauges the relative ability of an object's surface to emit energy by radiation), A is the surface area, σ is the Stefan-Boltzmann constant ($\sigma = 5.67 \times 10^{-8}$ J·s^{-1}·m^{-2}·K^{-4}), and T is the temperature of the object's surface. A simple example of emission of heat as radiant energy is an infrared bathroom heater where electric current is passed through a metallic element that reaches several thousand degrees and emits considerable thermal radiation.

All objects in the environment exchange radiant heat with each other and seek equilibrium temperatures. At high temperatures, many objects behave as "black body radiators" defined by their surface emissivity, $\varepsilon = 1$. The surface temperature of an object causes electromagnetic radiation to be emitted with a spectrum given by Planck's Distribution Law, equation 18, where the energy density is emitted by the surface of the object per wavelength per unit volume:

$$u(\lambda,T) = \frac{8\pi h c}{\lambda^5} \frac{1}{e^{\frac{hc}{\lambda k T}} - 1} \tag{18}$$

The terms in this equation are as follows:

- c: speed of light, (3×10^8 m/s).
- h: Planck's constant, (6.62×10^{-34} J·s).
- λ: wavelength of the emitted radiation, (m).
- k: Boltzmann constant, (1.38×10^{-23} J/K).
- T : surface temperature, (K).
- u(λ,T): spectral energy density, (J·m^{-3}·m^{-1}).

The surface of the sun behaves as a black body radiator[a] with a surface temperature of 5,778 K. For the sun, the Planck distribution of energy versus wavelength looks like that of Figure 12. The horizontal axis is the wavelength in units of meters and shows that peak energy occurs at a wavelength of about 5.02×10^{-7} meters or 0.502 microns (1 micron = 10^{-6} meters). This falls within the visible band (0.38 microns to 0.65 microns) and corresponds to the yellow color of our sun. The peak wavelength, equation 19, is given by Wien's Displacement Law:

$$\lambda_{max} = 2.8977685 \times 10^{-3} \ (m \cdot K) / T \tag{19}$$

This shows that as the temperature of an object increases, the amount of radiant energy released by the surface increases and the value of the peak wavelength becomes smaller.

---

[a] A black body is an idealized object that absorbs all electromagnetic radiation that falls on it. Since a black body is a perfect absorber of radiant energy, by the laws of thermodynamics it must also be a perfect emitter of radiation.
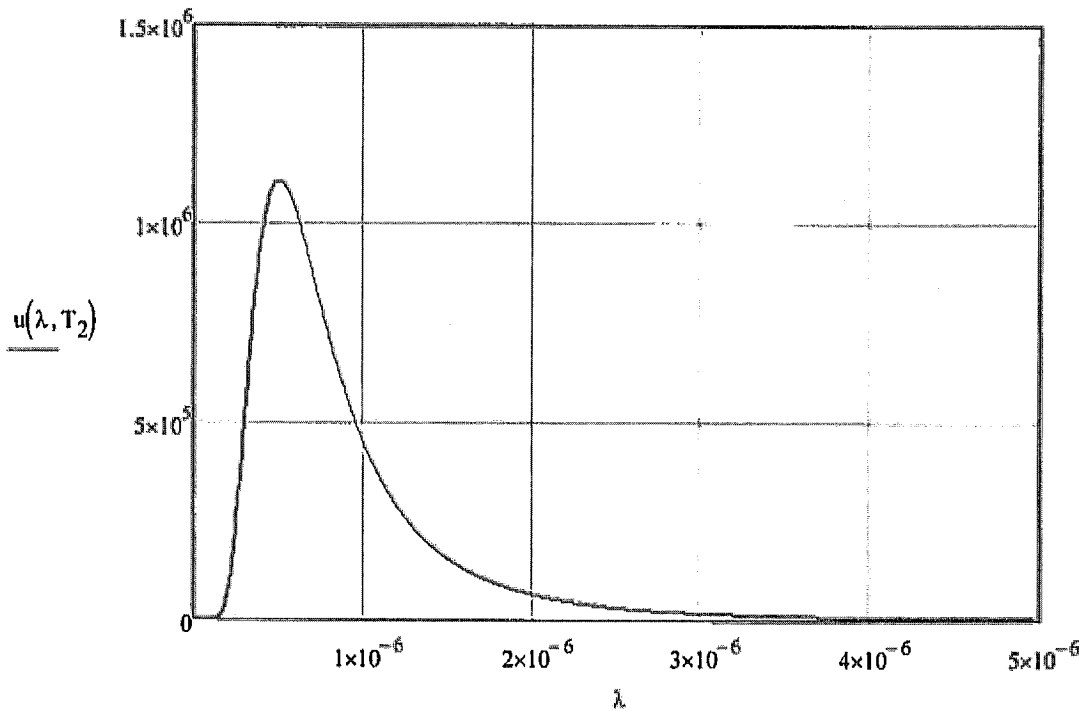
Figure 12. Energy Spectrum of the Sun at 5,778 K.

Application of Planck's Law to Hypersonic Vehicles.

As described in the theory of hypersonic fluid flow, any object moving through the atmosphere with an M > 1 will result in a shock wave emanating from the leading edge of the object. If the object has a blunt nose, such as a meteor entering the atmosphere, the shock will be detached from the surface. If we consider a spherical object moving through the atmosphere at hypersonic speed, as shown in Figure 13, the expected spectrum of emitted radiation can be computed. In this example, the altitude is assumed to be 10 km above the Earth's surface. At this altitude, the ambient static temperature is 223 K (−50° C), the pressure is 26.1% of sea level atmospheric pressure (see Appendix A for the properties of the U.S. Standard Atmosphere).
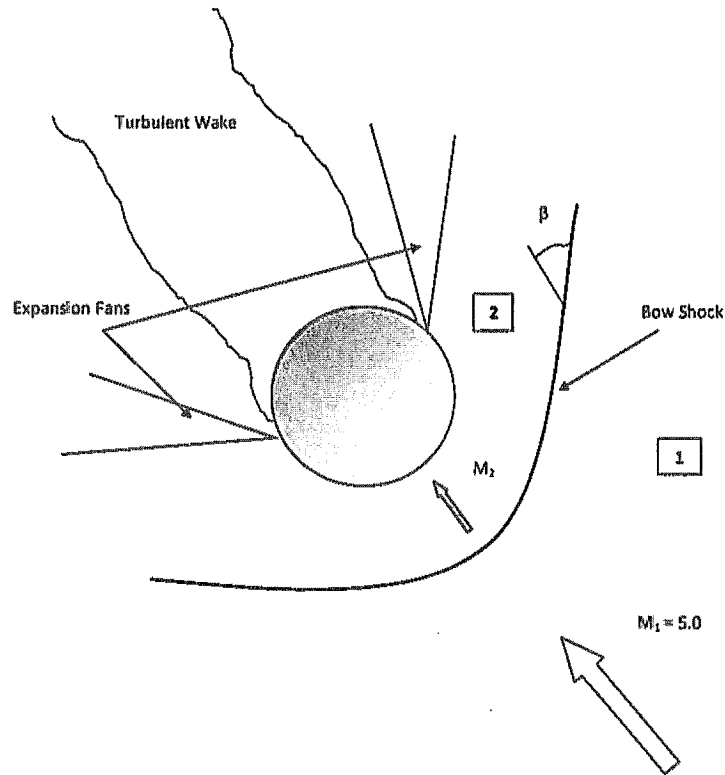
Figure 13. Hypersonic Flow Past a Sphere.

If the sphere in Figure 13 were traveling through the atmosphere at Mach 3, could we identify the speed of the sphere by the peak wavelength of the infrared radiation that it emits? From compressible aerodynamics relationships, conditions behind the bow shock, in region 2, can be calculated. We find that the peak static temperature would reach 597 K and the peak wavelength 4.85 microns. Figure 14 shows the expected infrared spectrum. For comparison, the spectrum for Mach 3.5 is also shown. In the figure, the wavelength has units of microns (i.e., 10^{-6} meter). As the Mach number increases, the peak temperature also rises while the peak wavelength decreases (shifts to the left). The higher the Mach number, the greater the amount of infrared energy emitted. For Mach 3.5, the peak wavelength is 3.92 microns. The energy difference between a Mach 3 and Mach 3.5 aircraft would be significant enough to detect with an infrared camera or FLIR (forward looking infrared) detector.
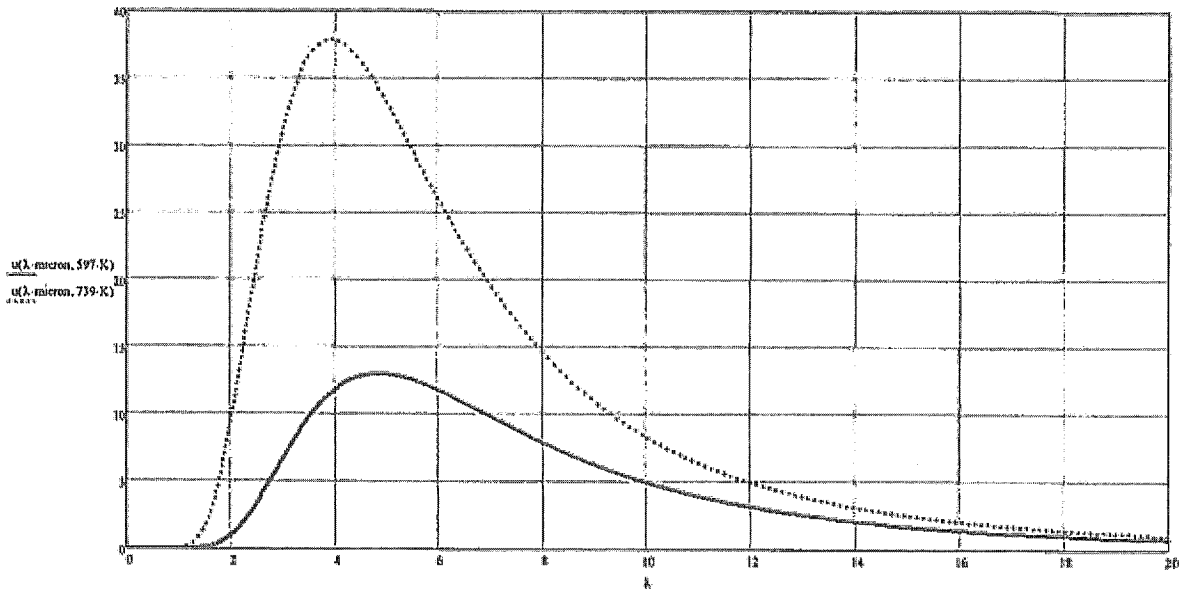
Figure 14. Infrared Energy Spectra for Mach 3 (red line) and Mach 3.5 (blue dashed line).

The peak wavelength changes for hypersonic aircraft with speeds that range from Mach 1 to Mach 100 are included in Figure 15. Satellite systems currently monitor 2.5- to 5-micron IR emissions and could detect aircraft with speeds as low as Mach 3. While Figure 15 plots the peak wavelength, aircraft at Mach 5 or higher have lower temperatures in the turbulent wake that would still be detectable. The peak temperatures are shown in Figure 16. Above 550 K, the perfect gas law cannot be used to accurately predict the peak temperature due to ionization and disassociation of molecules in the air. Figure 15 and Figure 16 use the "rule of thumb" described earlier in the theory of hypersonic vehicle flight to determine peak temperature and the corresponding wavelength.

Military satellite systems monitor infrared energy emitted by objects on the surface of the Earth. Kidd and Caldwell[20] reported on the use of IR systems for defense support in 1992 and highlighted the problems in resolving missile launches and wakes from background "clutter" caused by the infrared emissions from other objects on the surface of the Earth. Typical satellite IR systems detect energy between 2 and 5 microns. To verify that an object is an actual missile, the object must be detected in the 2.6- to 3.2-micron band, which corresponds to the emission from water vapor in the hot exhaust of a rocket. It must simultaneously be identified in the 4.1- to 4.8-micron range to differentiate the missile from background clutter. One problem encountered in missile detection involves the "glint" that occurs as aircraft at high altitude passing over land at night reflects sunlight to an overhead satellite. Computer software to discriminate signals from background heat combined with detection in the two different infrared bands helps to identify actual missile launches. FLIR (forward looking infrared) is also now used for atmospheric surveillance to detect objects in the 3- to 5-micron band and in the 5- to 14-micron band.

21

Peak Wavelength of Emitted Radiation

Typical Satellite IR Systems Measure Radiation from 2.5 to 5 microns.
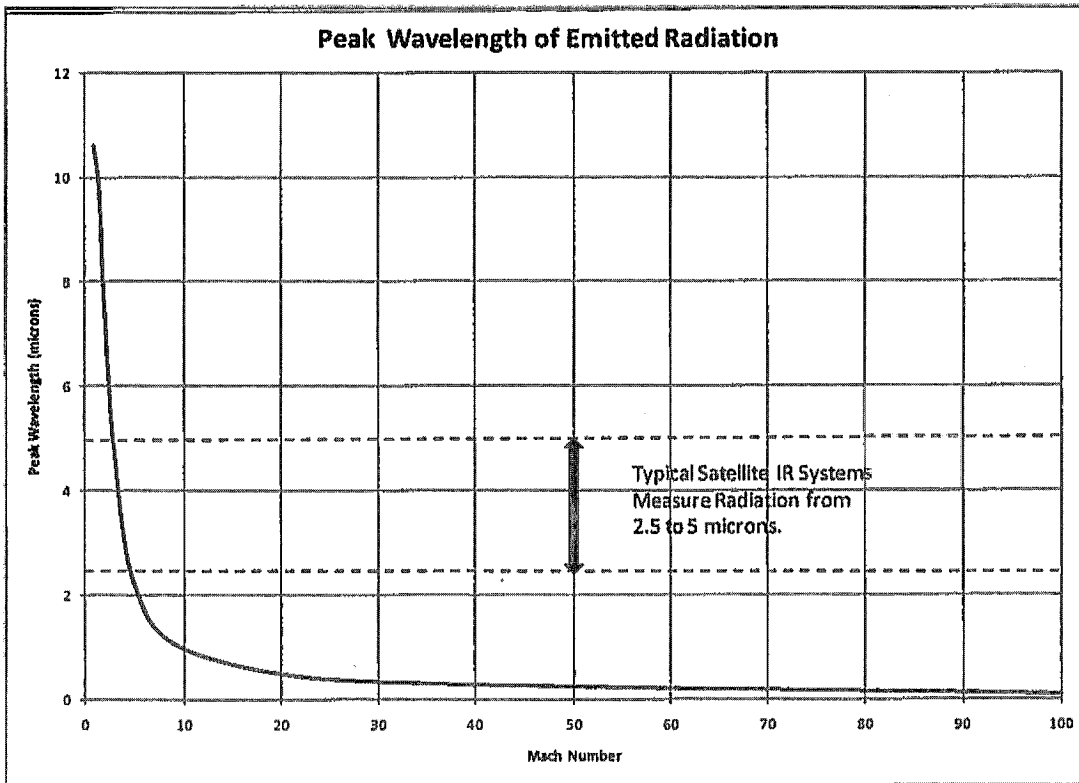
Figure 15. Peak Wavelength of the Infrared Radiation Emitted by Hypersonic Objects.

Temperature Downstream of a Normal Shock

Above 550 C (823 K), Ionization and Disassociation of Oxygen and Nitrogen Lead to Lower Temperatures in the Gases Downstream of the Bow Shock.
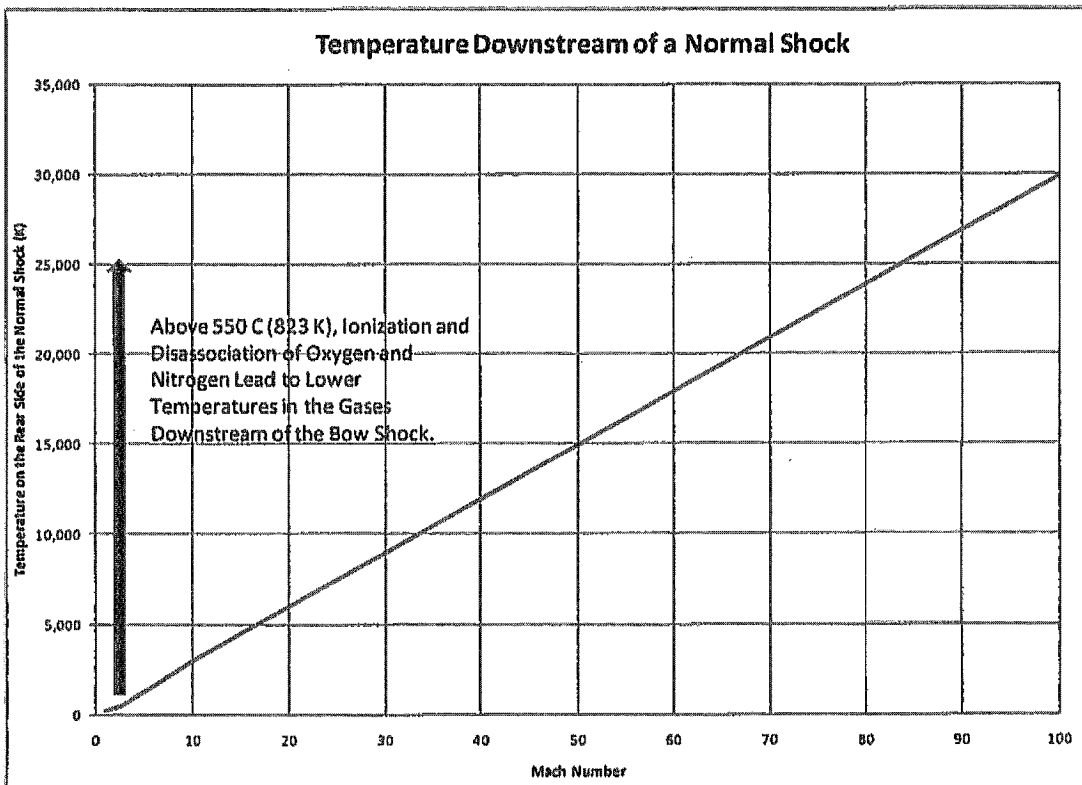
Figure 16. Peak Shock Layer Temperature for Hypersonic Objects.

22

Commercial and Governmental IR Systems

There is a long history in the United States of the usage of IR detectors to sense launches and to track the trajectory of ICBMs.[21] ARPA initiated studies of the possible use of IR detection of aircraft and missiles in the 1950s. Under their Defense Support Program (DSP), Joseph Knopaw studied the possible use of IR detectors in satellites to detect missiles and the hot exhaust plumes of ICBMs. Rand Corporation submitted a report in 1955 that outlined the detection of ICBM launches from satellites in Earth orbit. In 1956, the U.S. Air Force chose Lockheed as the lead designer with Joseph Knopaw as the project manager for Subsystem G, ICBM Attack Alarm System (WS-117L).

By 1958, control of the Air Force system shifted to ARPA (Advanced Research Projects Agency) as the MIDAS missile defense alarm system. The satellite IR detection system could alert the Strategic Air Command of possible Soviet missile launches 15 minutes earlier than the DEW system could. The first successful satellite launch occurred in 1960 with a 300-mile orbit. In 1963, MIDAS 9 with a 2,250-mile polar orbit succeeded in detecting nine missile launches using an 8-inch concentric telescope and an Aerojet-General IR detector.

In 1964, the Air Force launched the RJS-2 satellites into geosynchronous orbit over the equator. The MIDAS system was renamed the Defense Support Program in 1969 and an agreement between the United States and Australia provided communication to the constellation of MIDAS satellites from the Overseas Ground Station (OGS) in Australia and the Continental Ground Station (CGS) at the Buckley Air National Guard Station in the United States. Four Phase 1 Integrated Missile Early Warning Satellites (IMEWS) were launched between 1970 and 1973 followed by Phase 2 satellites from 1975 to 1977, the Multi-Orbit Satellite/Performance Improvement Modification (MOS/PIM) models from 1979 to 1984, two Sensor Evolutionary Development (SED) satellites from 1984 to 1987, and DSP-I satellites since 1989. The DSP satellites are designed for the global monitoring of ICBMs, SLBMs, and tactical missiles. Their operating life is 5 to 7 years, and they weigh approximately 5,000 lbs. With 6,000 IR telescopic detectors, these satellites monitor IR emissions between 2.7 and 4.3 microns. The 23rd, and last, DSP satellite was launched in November 2007.

The DSP system is capable of monitoring more than ICBMs. In 1972, the system detected a large meteor passing over several western states 94 km above the Earth. This meteor, moving at 18 km/s, was on a trajectory over Salt Lake City that would have done significant damage if it had impacted the Earth. In 1991, DSP satellites detected the launch of 88 Iraqi SCUD missiles. The DSP system is currently controlled under the ALERT (attack and launch early report to theater) system under the ALERT Control Center located at Shriever Air Force Base in Colorado. The current operational inventory is classified.

Other commercial IR detection equipment includes the Lucid Dimensions Spherical Detection System (SDS) using a 3D spherical sensor array.[22] This system is designed to track ballistic missiles, aircraft, and vehicles. Developed under an SBIR, this system can be mounted on ground-based vehicles, ships, or aircraft.

LIDAR

LIDAR, or "light detection and ranging," uses pulses of laser light directed toward a target. Reflected light is detected and, through the time of flight of the laser beam, the distance to the target can be computed. While LIDAR systems are similar in function to RADAR systems, the highly directional nature of the laser beam permits a very accurate determination of target distance. As an example, reflected panels left on the moon's surface by the Apollo astronauts are now used to accurately monitor the distance from the Earth to the moon using

LIDAR. By attaching a rotating mirror to vary the direction of the laser beam, it is possible to traverse the laser across surfaces to develop 3-D maps of objects using "imaging LIDAR." As an example, during the DARPA challenge held in the Nevada desert in 2005, autonomous automobiles used LIDAR to build a map of all objects in front of the vehicle and used it for collision avoidance and navigation. LIDAR systems have also been used to obtain accurate maps of the surface of mars from the Mars Orbiting Global Surveyer. LIDAR systems for meteorological studies are often mounted in aircraft and fired from the side of the fuselage to obtain a two-dimensional horizontal map of the atmospheric conditions.

A measurement technique known as Laser Doppler Velocimetry (LDV) uses the Doppler shift in the transmitted and reflected laser light to measure the velocity of the target and the properties of the air along the axis of the laser beam.

LIDAR systems using pulsed YAG lasers are capable of measuring many properties of air along the path of the laser beam. As shown in Figure 17, if a laser pulse is fired toward a distant target, light is reflected from particles in the atmosphere and this light is collected through a beamsplitter and directed to a photodetector. By knowing the time interval between generation of the laser pulse and the time that each reflected signal is received, the distance along the beam can be accurately determined for each data set. By recording this optical information as a function of time, using Raman spectroscopy, particle light scattering, and absorption theory, multiple properties of the air and particles in the air along the path of the laser can be measured as a function of distance from the transmitter. Particle density, velocity, and chemical species can be measured using pulsed LIDAR systems. Concentration of airborne gas species (oxygen, nitrogen), air temperature, and air velocity can also be measured in this fashion.
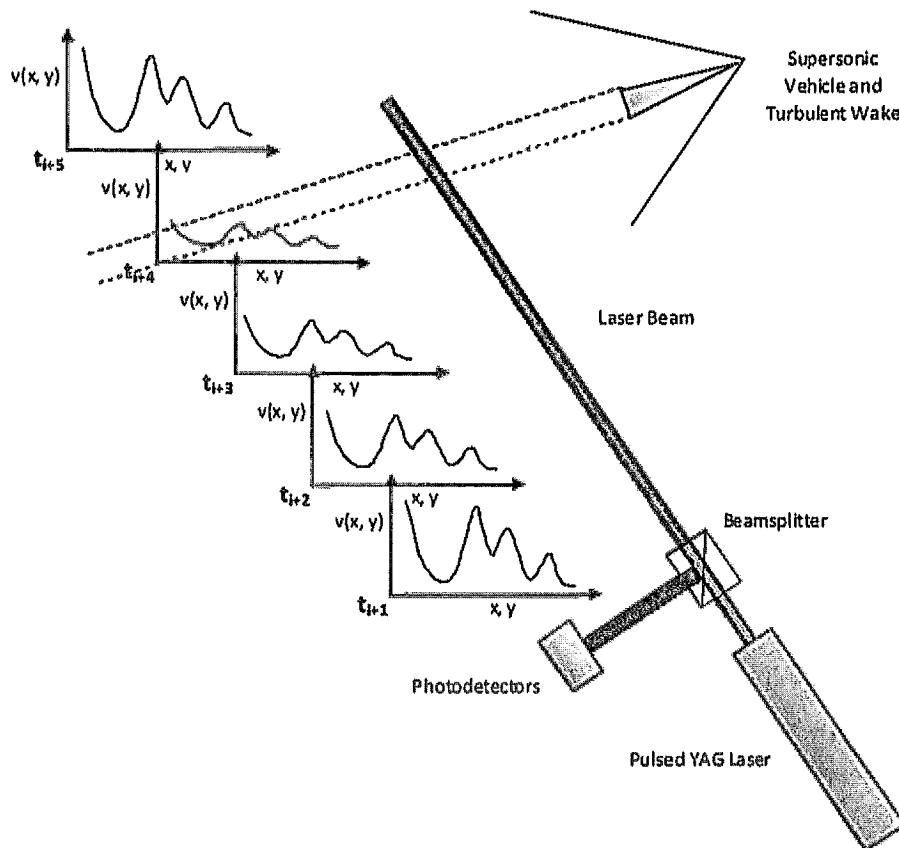

Figure 17. Schematic of a Pulsed LIDAR System.

LIDAR can be used to detect and monitor hypersonic objects in several ways. By using a micropulse laser, a LIDAR system could be used to scan the sky for supersonic airborne objects. LIDAR can also detect the presence of a hypersonic vehicle by measuring the air velocities in the long turbulent wakes that they leave in the atmosphere. Electro Optic Systems in Sydney, Australia,[23] has announced a laser tracking system that can track objects in low-Earth orbit that are as small as 100 mm (4 inches). These objects pose a risk to satellites and manned space vehicles due to their high velocities (~ 8 km/s). There are an estimated 200,000 such objects greater than 10 mm in size currently orbiting the Earth.

In the testing of hypersonic aircraft, a dedicated LIDAR system trained on the turbulent wake could measure the temperature and velocity distribution within the wake. This information can be used to design aircraft that would minimize detectability and increase vehicle reliability. The U.S. Army, for example, reported on the use of a LIDAR system to monitor atmospheric particulates from the erosion of nose-cones on Athena-H reentry missions at the White Sands Missile Range in New Mexico in 1973.[24] The LIDAR system monitored the path of the reentry vehicles at altitudes of 9.3 km and 14.3 km and determined the concentration of erosion products and ice particles along the laser beam path.

ACOUSTIC AND SEISMIC METHODS

Infrasound

Microphones can be used as a chronograph to measure the velocity of airborne objects. A supersonic aircraft generates a three-dimensional bow shock referred to as a "Mach cone." If the aircraft's Mach cone, which is actually a pressure pulse, sweeps over two microphones separated by a distance, the velocity of the aircraft can be measured. In Figure 18, two microphones can sense the dramatic pressure increase that occurs behind a shock wave and determine the velocity by dividing the microphone separation distance by the delay time.

Sound waves generated by the aircraft and the shock do not reach a terrestrial microphone until the Mach cone reaches the detector. The Mach cone has a half angle given by $\beta = arcsin\ (1/M)$, and this yields a method of detecting the aircraft altitude, H:

$$M = \sqrt{1 + \frac{D^2}{H^2}} \tag{20}$$

"Infrasound" refers to subaudible (< 100 Hz) sound waves that are generated by explosions, sonic booms, and rocket exhaust. Infrasound can be sensed by pressure transducers that detect the very small changes in atmospheric pressure that are induced by these events. The U.S. Air Force installed a network of infrasound stations around the country in the 1960s to detect the detonation of nuclear devices. Each station was composed of multiple pressure transducers so that the direction of the sound waves could be detected at the location of each station.

Mach Cone

$\beta = arcsin(1/M) = $ Mach Angle

Bow Shock

wake

Acoustic
Detector

D
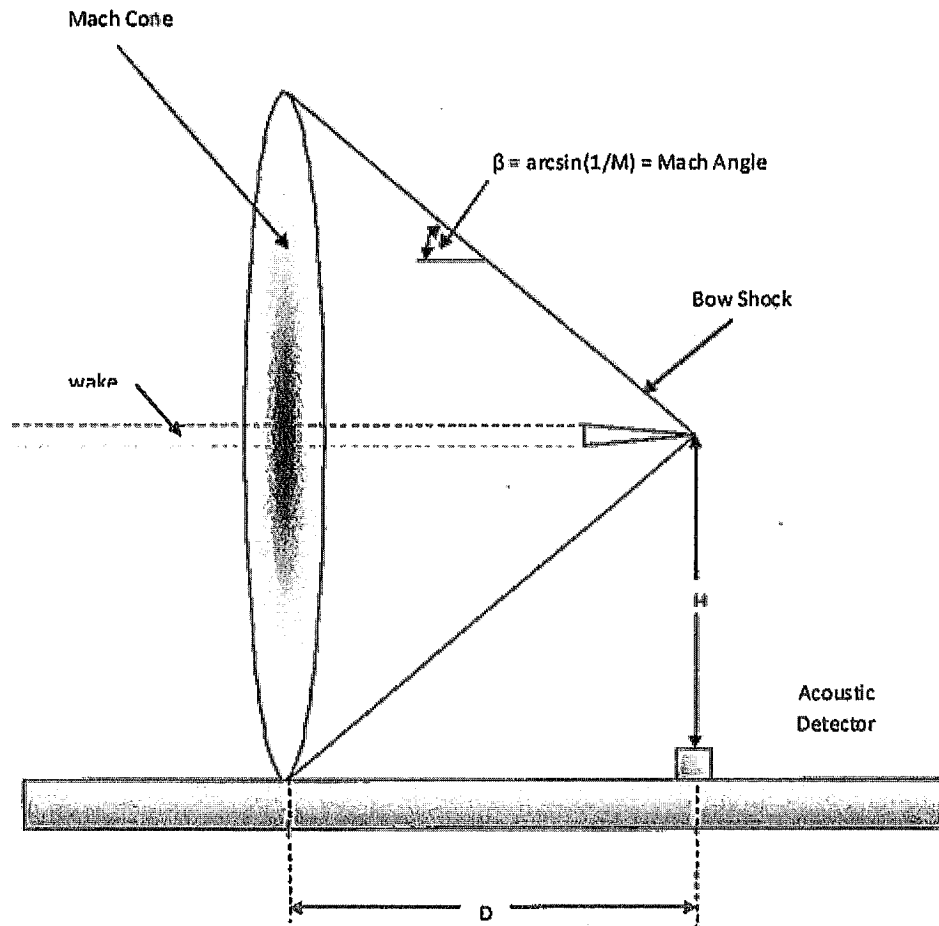
Figure 18. Mach Cone Generated by a Supersonic Object.

The Los Alamos National Laboratory still operates four of these stations that were installed in 1983 at various locations in the United States.[25] These infrasound detector stations are relatively inexpensive and are easy to maintain. While they have not yet been used to sense nuclear detonations, they do detect sonic booms, and they were responsible for identifying and tracking two large bolides, or brilliant meteors, that entered the Earth's atmosphere in 2000 and 2001. While capable of sensing meteors as small as a baseball, in 2001, a large bolide entered the Earth's atmosphere over the Pacific Ocean and exploded near Baja California. The bolide was estimated to have a 3.6-meter diameter and exploded with the energy of 6,000 tons of TNT.

Even a single infrasound station can track a meteor. On 4 October 1996, a station in Colorado observed a meteor near Bakersfield, California.[26]

Another infrasound station network includes the International Monitoring System, a network of 321 stations around the world designed to monitor explosions that would represent violations of the Comprehensive Nuclear Test Ban Treaty. Although this network may be a useful worldwide resource for the detection of meteors, reentry vehicles, and hypersonic flights, its use in the detection of nuclear explosions is dubious given the circumstances of November 1999. During this event, a sonic boom was monitored in the skies above northern Germany. The information provided by the network could not differentiate between a meteor and a nuclear explosion.

Infrasound stations, or observatories, could also be used to monitor the acoustic signature of meteors or supersonic aircraft based on their shock waves or the disturbances caused by their turbulent wake. Some meteors, for example, produce subsonic sound from 1 to 5 Hz for several minutes during their flight through the atmosphere. This data could be developed to identify the speed, altitude, and type of object moving through the atmosphere.

Seismic

When a sonic boom is generated by a meteor or an aircraft, the sound waves pass through the atmosphere at the speed of sound in air at about 343 m/s. Infrasound stations pick up the pressure variations caused by the shock wave many minutes after the event occurred, depending upon the distance between the supersonic object and the station. When a Mach cone generated by a shockwave strikes the ground as shown in Figure 18, the pressure pulse is propagated into the ground and travels as a high-speed N-wave at a velocity far exceeding the speed of sound in air.

Ground-based vibrations caused by sonic booms have been detected by seismic sensors originally designed to detect earthquakes as documented by Cates and Sturtevant.[27] Caltech and the U.S.G.S. operate 200 seismographic stations throughout Southern California as part of the TERRAscope seismic network. The network employs detectors that can sense ground vibration between 1 and 20 Hz.

The network was actually used to detect the sonic boom and pressure vibration induced by the flight of supersonic aircraft and reentry vehicles. On 9 December 1993, the network successfully detected the flight of an SR-71 flying over Edwards Air Force Base at a maximum speed of Mach 3.2. On 30 January 1992, the network was also used to detect the reentry of the space shuttle Discovery, STS-42, over the Pacific Ocean and landing at Edwards Air Force Base.

Another Discovery landing on the west coast was monitored by 66 seismic stations in Washington and Oregon. The shuttle was monitored by this seismic network for 500 km of its trajectory through the atmosphere. The seismic data from these stations showed the hyperbolic shape of the Mach cone as it impacted the surface of the earth. The angle of the Mach cone showed that the shuttle was traveling at Mach 14, corresponding to an altitude of 55 km.

One interesting investigation that involved the use of these seismic arrays involved mysterious sonic booms heard over Southern California in 1991 and 1992. By using data from the TERRAscope array, the source of these disturbances was traced to two F-4 Phantom aircraft flying over Edwards Air Force Base at speeds near Mach 1.

Since the TERRAscope array is designed to detect seismic activity, including earthquakes and volcanoes, the detection of meteors and supersonic aircraft generate unwanted data. Caltech has been adding atmospheric pressure transducers to its seismic network to detect and remove airborne signals from the seismic data. Conversely, by combining the infrasound network data operated by the Los Alamos National Laboratory with data from seismic arrays, data from explosions, volcanic eruptions, and other terrestrial sources can be eliminated from infrasound data to better detect the presence of meteors, reentry vehicles, and supersonic aircraft.

Chapter 4: Vision of Progress Over the Next 30 Years

While there are several methods that can be used to sense high-speed supersonic objects, technology changes in aircraft will generate the need for newer detection and tracking techniques. Listed below are five important categories of objects capable of hypersonic speeds. Over the next 30 years, the ability to reliably and accurately detect them will be critical.

- Space Debris – Technology is currently available to detect space debris using RADAR and cameras. Novel methods using coronographs[28] during daylight have been shown to detect the reflected light from millimeter-size debris particles in orbit, and existing telescopes are capable of detecting meteors that pose a risk to Earth. Space debris reentering the Earth's atmosphere can reach speeds of over 17,000 miles per hour or Mach 23.

- Reentry Craft – The highest recorded speed for any manmade vehicle was the Apollo 10 reentry capsule in 1969. It reached a velocity of 24,790 mph, or Mach 36. Reentry vehicles are currently monitored by ground-based telescopes and RADAR and through satellite imagery.

- Meteors – The systems used to monitor missiles and satellites based on RADAR and optical devices can currently detect and track meteors entering the Earth's atmosphere. Further development of acoustic and radio detection techniques should be pursued over the next 30 years.

- Missiles – The Cold War generated the need for equipment to monitor hostile missile launches, to track their path, and to estimate the location of their targets based on ballistic trajectories. The United States Space Surveillance Network, for example, is composed of a worldwide collection of RADAR, electro-optical detectors, and passive RF devices that can track satellites, missiles, and aircraft. They maintain an inventory of satellites in Earth orbit and, through the Space Surveillance Telescope program (SST), asteroids and other faint objects in space are detected and tracked. GEODSS (Ground-Based Electro-Optical Deep Space Surveillance) telescopes monitor space at 3 different locations around the globe with high enough resolution to detect a basketball 20,000 miles from the Earth. Continued vigilance from governments around the world will likely increase the development of technology to detect and track high-speed objects in the atmosphere and in space over the next 30 years with an emphasis on RADAR and optical detection.

- Hypersonic Aircraft – Over the next three decades, hypersonic aircraft development will likely spur an increased need for new technology to detect their presence. While the X-15 rocket plane exceeded Mach 6 (4,520 mph) as early as 1967, continued development of high-speed aircraft will continue to meet needs in the following areas:

    o SSTO (Single Stage to Orbit) – Long the dream of NASA and space exploration enthusiasts, technology has been under development to replace the Space Shuttle using aircraft that can take off from a conventional runway and attain low-Earth orbit. The X-43A scram jet, part of NASA's Hyper X Program and fueled by hydrogen fuel was successfully tested in 2004. This aircraft is capable of 7,000 mph or Mach 9.8 flight.

28

o <u>Manned military jet fighters</u> – The fastest military jet is the MIG-25 Foxbat at 2,115 mph (M = 3). The fastest U.S. jet is the F-15 at 1,875 mph (Mach 2.6). Current U.S. efforts are concentrating on unmanned vehicles, such as the X-43A.

o <u>Surveillance aircraft</u> – The SR-71a "Blackbird" achieved 2,056 mph (Mach 3.3) in 1976 using an air-breathing engine. Its rumored replacement, the SR-91 Aurora, would have been capable of Mach 6. In 2008, the U.S. Air Force entered into an agreement to design a Mach 6 unmanned "blackswift" aircraft using a scramjet.

o <u>Passenger jets</u> – The current record holder is the Tupolev Tu-144 "charger" at 1,553 mph (Mach 2.15). Reaction Engines Limited has proposed the A2 hypersonic passenger liner using liquid hydrogen to fuel the aircraft and to cool the wings and fuselage. This aircraft is expected to achieve Mach 5. In 2000, Russia and the People's Republic of China entered into a 25-year agreement to develop the Leninetz AYAKS hypersonic transport plane using kerosene fuel and a variety of techniques to attain Mach 8 to 10. An MHD (magnetohydrodynamic) engine is used to further accelerate combustion products produced by the engine. Lasers and RF generators are employed to disrupt the bow shock, reducing drag and doubling the velocity of the vehicle.

o <u>Stealth missiles</u> – The USAF Falcon Project planned for building a Mach 6 HTV-3V "Blackswift" platform but was cancelled in 2008. The NASA X-51 scramjet vehicle is based on the Falcon scramjet and is scheduled for testing in 2010. This vehicle is capable of Mach 7+.

DETECTABILITY OF NEW HYPERSONIC AIRCRAFT

While conventional RADAR and optical systems may be able to track existing vehicles, future aircraft capable of Mach 8 and above are now being designed and tested. New propulsion technology and drag reduction techniques also offer new ways to detect such aircraft. Based on a review of hypersonic vehicle detection and tracking, four recommendations are made for research and technology development over the next 30 years to increase the detectability of hypersonic objects passing through the Earth's atmosphere.

Recommendation #1 – Build a Database of the Wake Characteristics for Existing Aircraft

There is considerable information about the aircraft contained within the turbulent wake that trails it. The wake provides an indication of the vehicle's path and its current bearing. By analyzing the Strouhal eddy formation, it is possible to ascertain its velocity and hydraulic diameter. The wake can also provide information on the chemical combustion products that can be obtained through LIDAR and can indicate the fuel used by the aircraft. Some aircraft, such as the X-43A and the proposed Reaction Engines Limited A2, use hydrogen as the fuel, so the absence of carbon molecules in their turbulent wakes could aid in their identification.

Authors Mark Garnet and Aaron Altman from the University of Dayton[29] proposed the development of a database of turbulent wake data for conventional aircraft to allow their identification. They point out that, although the aircraft may be designed for stealth, their wakes cannot be hidden. They presented data on the unique characteristics that can be used to identify the wakes generated by the F-15, F-16, F-18, and B-52. They also point out the

need for computational modeling of hypersonic wakes to predict the characteristic signature of new, unknown aircraft.

A hypersonic vehicle database of wake characteristics for existing aircraft should be developed based on optical and Doppler RADAR data. Doppler RADAR provides information on turbulent intensities and eddy formation within the wake. Computational fluid mechanics models of hypersonic wakes have been done since the early 1960s, such as the work done by Zieberg and Bleich.[30] Such modeling work should continue capitalizing on the increasing computer performance that will be available during the next 30 years.

Recommendation #2 – Exploit the Detectability of Hypersonic Aircraft Based on the Features That Allow Them To Fly Efficiently at High Speeds

Several new propulsion systems for hypersonic aircraft will be tested over the next 30 years. These include pulsed detonation engines (PDE) successfully tested in 2008 by the Air Force Research Laboratory and Innovative Scientific Solutions, Inc. over the Mojave Desert. While these engines are capable of Mach > 6, they have one characteristic that makes them very detectable. The pulsed detonation of combustible fuel creates a wake with periodic bulges referred to as "donuts on a rope." As mentioned earlier, measurements of the turbulent wake behind hypersonic aircraft can be used for detection, identification, and tracking.

The AYAKS hypersonic transport plane under development in Russia uses an MHD engine, lasers, and RF generators to decrease aircraft drag. The lasers and RF ionize the air ahead of the aircraft, creating a plasma to disrupt the bow shock and significantly reduce aerodynamic drag. Drag reduction allows the aircraft to double its maximum speed. The RF and laser emissions from this aircraft can possibly be used to detect the aircraft in flight from ground-based antenna or telescopes or from satellites. The MHD engine also generates electromagnetic radiation that can possibly be detected.

Every new propulsion or drag reduction system under development will have some characteristic that may make it more detectable from the ground or from satellite. The Aerospike engine proposed for the SSTO and under development by Rocketdyne and Garvey Spacecraft involves the use of a novel virtual Laval nozzle that is external to the engine. The IR emissions from an Aerospike engine may increase its detectability.

Recommendation #3 – Explore the Detection of Vehicles Designed To Be Undetectable

Over the next 30 years, hypersonic cruise missiles will have the ability to travel at speeds of up to Mach 8 decreasing the chances of being detected or defeated by antimissiles. The unmanned NASA X-51 tested in 2010 is capable of greater than Mach 7 (over 4,000 mph), for example, and is designed to be launched from a B-52. The DARPA/USAF Falcon Project has resulted in the testing of the HTV-2 at Mach 6.7 over the Pacific Ocean, designed as a hypersonic cruise vehicle.

Efforts to disguise aircraft through the use of novel vehicle shapes and stealth materials can also increase their detectability in other ways. Golovitichev and Hansson presented a paper in 1999[31] that stated the following:

> "The concentrated energy drag reduction concept has proven to be effective for the cruise range vehicles, preventing the missile deceleration with the benefit that the spike "products" could envelope the missile in a film of ionized gas which would be impervious to RADAR pulses, thereby rendering it electronically "invisible". The infra-

red penalty at close range would be significantly offset by the high speed of the flight."

This discussion about the AJAX engine concerned the generation of ion combustion products that would be further accelerated by an MHD (magnetohydrodynamic drive). The increased number of various carbon-based molecules in the wake of this aircraft could be detected using LIDAR. The increased temperature near the surface of this aircraft would also increase its detectability due to increased emission of infrared radiation. For AJAX (AYAK) vehicles, development of enhanced LIDAR systems and IR detectors should proceed over the next 30 years to increase their detection and tracking.

Recommendation #4 – Explore the Development of Novel Detectors

One characteristic of hypersonic flight (M > 5) is the ionization of air in the region downstream of the bow shock and the disassociation of oxygen and nitrogen at very high speeds. When electrons recombine with ions generated by the shock, they emit electromagnetic radiation that can be detected. This radiation extends from the visible range, as evidenced by the glowing trail left by meteors entering the Earth's atmosphere, but the emitted radiation also extends into the ultraviolet and x-ray range. Although such electro-optical sensors are likely part of the existing DARPA/USAF space surveillance system, telescope systems that monitor the UV range should be developed, along with x-ray detectors capable of monitoring the atmosphere.

Hypersonic objects passing through the atmosphere disassociate nitrogen and oxygen which recombine in the object's turbulent wake. During recombination, new molecules are created, including NO, NO_2, ionized O and N, and combustion products.[32] LIDAR can detect the presence and concentration of these compounds in vehicle wakes and improved LIDAR systems should be a priority.

As hypersonic objects pass through the atmosphere, the object becomes ionized with a significant positive charge. Technology should be developed to sense the flight of objects with an electrostatic charge as they pass through the atmosphere.

SUMMARY

Each detection system discussed in the previous section has both benefits and problems. A comparison of the various detection techniques is shown in Figure 19 based on their ability to detect specific properties, relative cost, and accuracy.

Infrared detection systems and multispectral cameras installed on satellites, such as the KH-11, provide surveillance of large portions of the Earth for possible missile launches, reentry vehicle trajectories, meteor wakes, and hypersonic vehicles. RADAR systems based on satellites, ships, and aircraft can detect the position and velocity of such hypersonic objects at varying range. AWACS, for example, can detect objects at up to 370 km with a resolution of 0.5 meters. TRADEX can track up to six objects at a distance of 1,400 km with an accuracy of 3 meters and a velocity resolution of 0.01 m/s.

31

Detection Method				Properties Detected				Availability			Useful for Detection of:		
				Distance To Target	Velocity	Altitude	Whole Sky Or Directed	Commercially Available	Existing Network	Expense	Meteor Detection	Reentry Vehicles	Aircraft
Electromagnetic													
	Radar			x	x	x	Both	x	x	Modest	x	x	x
	Radio Reflection Detection						Whole Sky		x	Low	x	x	
Optical													
	Sky Cameras, Photographic						Whole Sky	x	x	Low	x	x	x
	Infrared				possible		Both	x		Modest	x	x	x
	Lidar			x	x		Directed	x		Medium	x	x	x
	Chronograph				x		Directted			Low			
Acoustic and Seismic													
	Infrasound			x	x		Whole Sky	x	x	Low	x	x	x
	Seismic			x	x		Whole Sky		x	Modest	x	x	x

Figure 19. Comparison of Detection Technology for Hypersonic Objects.

LIDAR systems provide detailed information on velocity, temperature, particle velocity, and atmospheric composition along the path of the laser beam that can be used to interrogate vehicle wakes and exhaust plumes. Seismic and infrasound systems continuously operate and can provide information on the path followed by a high-speed aircraft or object by tracking its sonic boom and low-frequency acoustic signature. Finally, optical cameras aimed toward the Earth provide valuable information on hypersonic object tracks by recording their tracks. Aimed toward space, optical cameras are tracking asteroids and other spaceborne objects that may enter the atmosphere as a meteor posing a risk.

Appendix A: MathCad Program Used To Estimate Hypersonic Vehicle Surface Temperature

Modeling of the Thermodynamic Properties Of Airflow about Hypersonic Vehicles

I. Purpose: Compute the properties across the bow shock of a hypersonic vehicle moving through the earth's atmosphere.

A. Define the Aircraft Velocity

$V := 3300 \cdot MPH$ *Vehicle Velocity.*

$H := 10 \cdot km$ *Vehicle Altitute.*

Note that the Karman Level corresponds to 100 km altitude where the atmosphere essentially ends.

B. Compute the Mach number for the Vehicle

$T_{atm}(H) = 222.986 \, K$

$a := \sqrt{\gamma \cdot R_{air} \cdot T_{atm}(H)}$ $a = 299.326 \, \dfrac{m}{s}$

$M_1 := \dfrac{V}{a}$ $M_1 = 4.929$

C. Compute the Stagnation Properties Upstream of the Bow Shock

$T_1 := T_{atm}(H)$ $T_1 = 222.986 \, K$

$T_{o1} := T_1 \cdot \left(1 + \dfrac{\gamma - 1}{2} \cdot M_1^2\right)$ $T_{o1} = 1.306 \times 10^3 \, K$

$p_1 := p_{atm}(H)$ $p_1 = 0.261 \cdot atm$

$p_{o1} := p_1 \cdot \left(1 + \dfrac{\gamma - 1}{2} \cdot M_1^2\right)^{\frac{\gamma}{\gamma - 1}}$ $p_{o1} = 126.94 \cdot atm$

D. Compute the Properties on the Downstream Side of the Bow Shock at the Nose

1. The following functions describe the change in properties across a normal shock.

$$M_2(M_1) := \sqrt{\frac{1 + \frac{(\gamma - 1)}{2} \cdot M_1^2}{\gamma \cdot M_1^2 - \frac{(\gamma - 1)}{2}}} \qquad \rho_{ratio}(M_1) := \frac{(\gamma + 1) \cdot M_1^2}{2 + (\gamma - 1) \cdot M_1^2}$$

$$P_{ratio}(M_1) := 1 + \frac{2 \cdot \gamma}{\gamma + 1} \left(M_1^2 - 1 \right) \qquad u_{ratio}(M_1) := \frac{1}{\rho_{ratio}(M_1)}$$

$$T_{ratio}(M_1) := \left[1 + \frac{2 \cdot \gamma}{\gamma + 1} \cdot \left(M_1^2 - 1 \right) \right] \cdot \left[\frac{2 + (\gamma - 1) \cdot M_1^2}{(\gamma + 1) \cdot M_1^2} \right]$$

a. Stagnation temperature and pressure ratios.

$$T_{o.ratio}(M_1) := 1.0$$

$$P_{o.ratio}(M_1) := P_{ratio}(M_1) \cdot \frac{\left[1 + \frac{\gamma - 1}{2} \cdot \left(M_2(M_1) \right)^2 \right]^{\frac{\gamma}{\gamma - 1}}}{\left(1 + \frac{\gamma - 1}{2} \cdot M_1^2 \right)^{\frac{\gamma}{\gamma - 1}}}$$

2. Compute the properties across a normal shock for this problem.

$$M_2 := M_2(M_1) \qquad\qquad M_2 = 0.416$$

$$T_2 := T_1 \cdot T_{ratio}(M_1) \qquad\qquad T_2 = 1.263 \times 10^3 \, K$$

$$P_2 := P_1 \cdot P_{ratio}(M_1) \qquad\qquad P_2 = 7.447 \times 10^5 \, Pa$$

$$P_{o2} := P_{o1} \cdot P_{ratio}(M_1) \qquad\qquad P_{o2} = 3.624 \times 10^8 \, Pa$$

$$T_{o2} := T_{o1} \cdot T_{ratio}(M_1) \qquad T_{o2} = 7.396 \times 10^3 \, K$$

$$\beta := asin\left(\frac{1}{M_1}\right) = 11.707 \, deg \qquad \textit{This is the Mach angle for a blunt-nosed object.}$$

E. Compute the Peak Wavelength of Emitted Infrared Energy

    1. Using Wien's Displacement Law, compute the peak wavelength of emitted radiation.

$$b := 2.8977685 \, 10^{-3} \cdot m \cdot K$$

$$\lambda_{max} := \frac{b}{T_2} \qquad\qquad \lambda_{max} = 2.295 \times 10^3 \cdot nm$$

$$\lambda_{max} = 2.295 \, micron$$

$$\lambda_{max} = 2.295 \times 10^{-6} \, m$$

    2. Using Planck's Law, compute the distribution of emitted energy with wavelength.

$$u(\lambda, T) := \frac{8 \cdot \pi \cdot h \cdot c}{\lambda^5} \cdot \left(\frac{1.}{e^{\frac{h \cdot c}{\lambda \cdot k \cdot T}} - 1}\right)$$

Spectral Energy Density for a Black Body Radiator in energy per unit volume per unit wavelength.
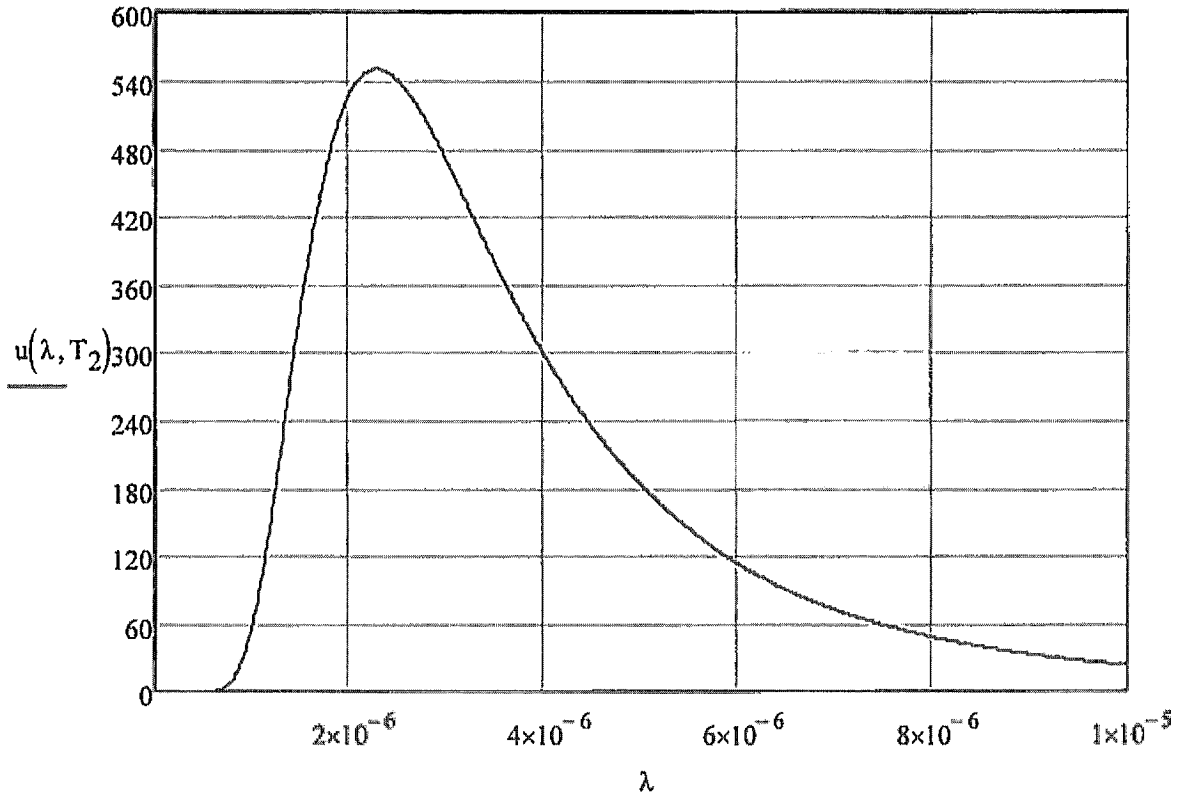
II. Definition of Units

$$MPH \equiv \frac{mile}{hr}$$

$h \equiv 6.62606896 10^{-34} \cdot J \cdot s$ *Planck's Constant.*

$k \equiv 1.3806504 10^{-23} \cdot \frac{J}{K}$ *Boltzmann Constant.*

$c \equiv 2.99792458 10^{8} \cdot \frac{m}{s}$ *Speed of light in a vacuum.*

III. Properties of Atmospheric Air

A. Fundamental properties.

$\gamma \equiv 1.4$ *Ratio of specific heats for air.*

$R_{air} \equiv 287 \cdot \frac{J}{kg \cdot K}$ *Gas constant for air.*

B. U.S. Standard Atmosphere

1. The raw data is included in the matrix "data."

2. Functions will be developed from a cubic spline interpolation of the data.

$$data \equiv csort(data, 0)$$

$$height \equiv \left(10^3 data\right)^{\langle 0 \rangle} \cdot m$$

$$pressure \equiv \left(10^3 data\right)^{\langle 1 \rangle} \cdot Pa$$

$$temperature \equiv data^{\langle 2 \rangle} \cdot K$$

$$density \equiv data^{\langle 3 \rangle} \cdot \frac{kg}{m^3}$$

$$pressure_{fit} \equiv cspline(height, pressure)$$

37

0.000	101.32	288	1.226
0.305	97.72	286	1.191
0.610	94.21	284	1.156
0.914	90.81	282	1.122
1.219	87.51	280.1	1.089
1.524	84.31	278.1	1.056
1.829	81.2	276.1	1.025
2.134	78.18	274.1	0.994
2.438	75.26	272.2	0.963
2.743	72.43	270.2	0.934
3.048	69.68	268.2	0.905
3.353	67.02	266.2	0.877
3.658	64.44	264.2	0.850
3.962	61.94	262.2	0.823
4.267	59.52	260.3	0.797
4.572	57.18	258.3	0.771
4.877	54.92	256.3	0.747
5.182	52.72	254.3	0.722
5.486	50.6	252.3	0.699
5.791	48.45	250.4	0.674
6.096	46.56	248.4	0.653
6.401	44.64	246.4	0.631
6.706	42.79	244.4	0.610
7.010	41	242.4	0.589
7.315	39.27	240.5	0.569
7.620	37.6	238.5	0.549
7.925	35.99	236.5	0.530
8.230	34.43	234.5	0.512
8.534	32.93	232.5	0.493
8.839	31.48	230.5	0.476
9.144	30.09	228.6	0.459
9.449	28.74	226.6	0.442
9.754	27.45	224.6	0.426
10.058	26.2	222.6	0.410
10.363	25	220.6	0.395
10.668	23.84	218.7	0.380
10.973	22.73	216.7	0.365
11.278	21.66	216.5	0.349
11.582	20.65	216.5	0.332
11.887	19.68	216.5	0.317
12.192	18.75	216.5	0.302
12.497	17.87	216.5	0.288
12.802	17.04	216.5	0.274
13.106	16.24	216.5	0.261
13.411	15.47	216.5	0.249
13.716	14.75	216.5	0.237
14.021	14.06	216.5	0.226
14.326	13.4	216.5	0.216
14.630	12.77	216.5	0.206
14.935	12.17	216.5	0.196
15.240	11.6	216.5	0.187
16.180	10	216.3	0.161
18.442	7	216.3	0.113
20.576	5	217.2	0.080
23.849	3	220.3	0.047
26.481	2	223.1	0.031
31.055	1	227.6	0.015
100	0	0	0

data

$$\text{temperature}_{\text{fit}} \equiv \text{cspline(height , temperature)}$$

$$\text{density}_{\text{fit}} \equiv \text{cspline(height , density)}$$

3. These functions provide atmospheric pressure, temperature, and density for the U.S. Standard Atmosphere from 0 to 100 km in height.

$$p_{\text{atm}}(h) \equiv \text{interp}\left(\text{pressure}_{\text{fit}}, \text{height , pressure , h}\right) \qquad \text{Pressure (Pa)}.$$

$$T_{\text{atm}}(h) \equiv \text{interp}\left(\text{temperature}_{\text{fit}}, \text{height , temperature , h}\right) \qquad \text{Temperature (K)}.$$

$$\rho_{\text{atm}}(h) \equiv \text{interp}\left(\text{density}_{\text{fit}}, \text{height , density , h}\right) \qquad \text{Density (kg/m\^3)}.$$
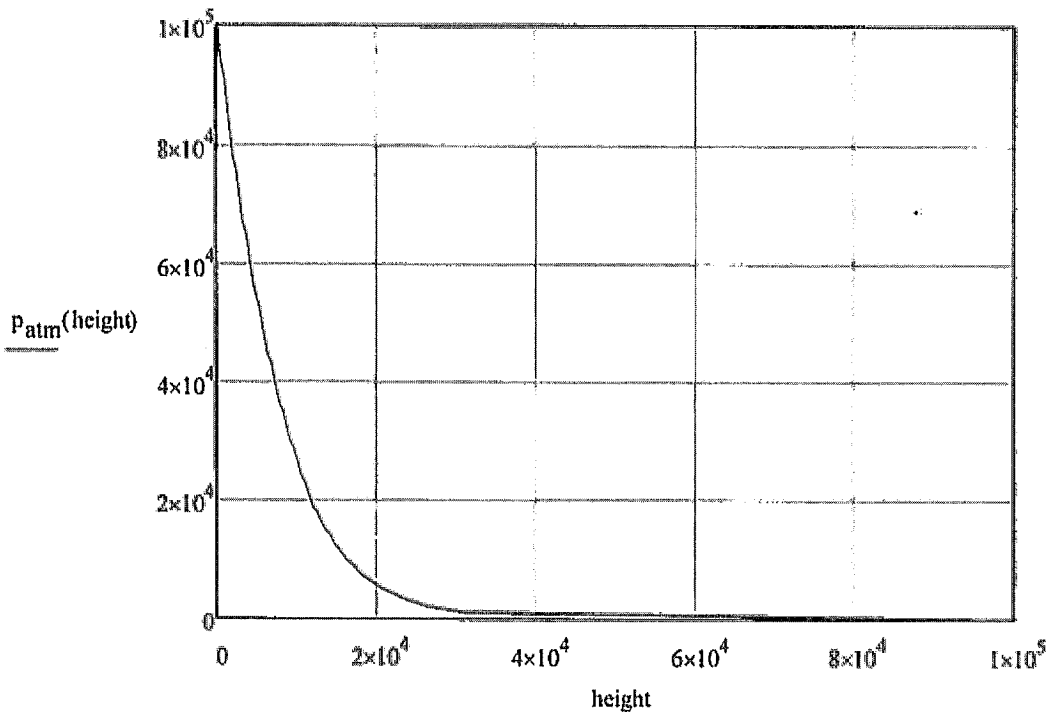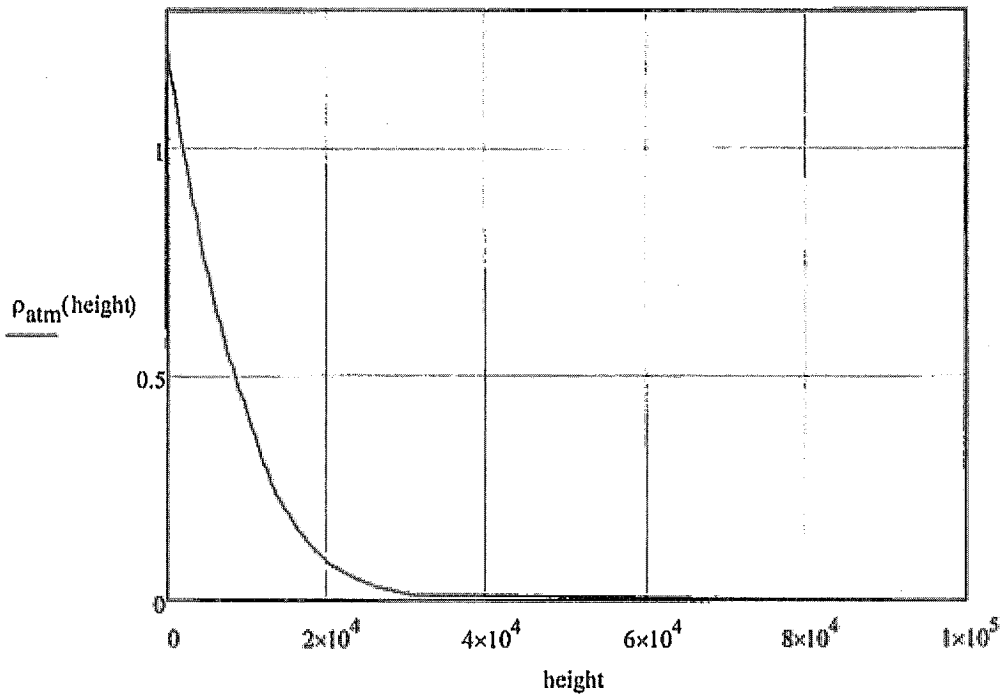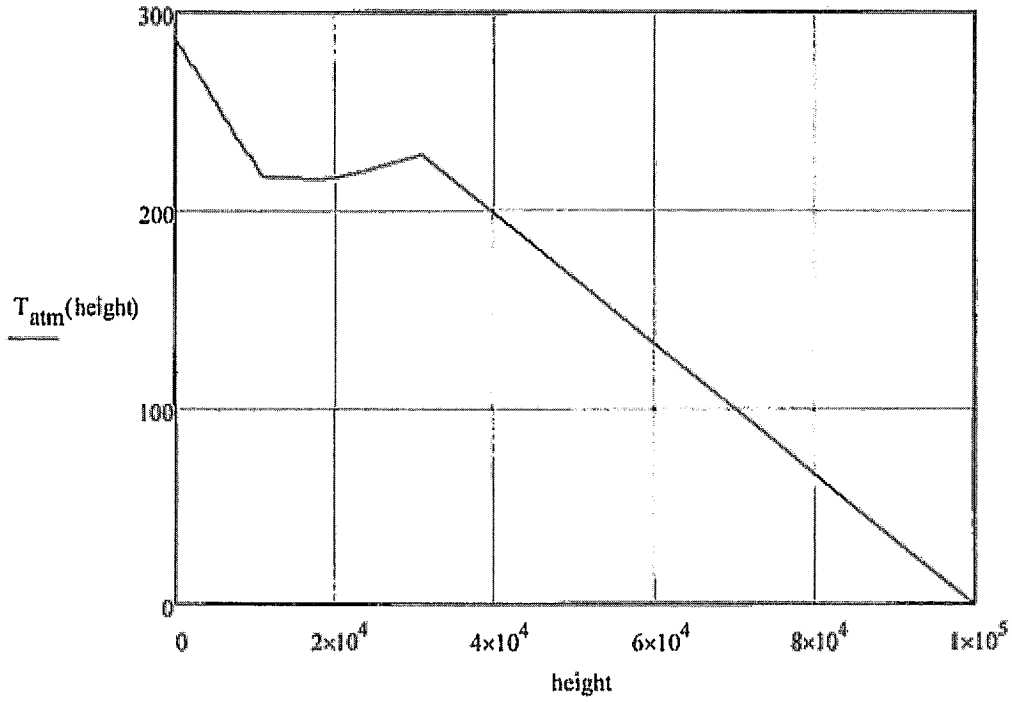
[1] Dyrud, L. P., et al, "Meteor velocity determination with plasma physics," Atmospheric Chemistry and Physics, 4, pp. 817-824, 2004.

[2] Anderson, John D., Modern Compressible Flow, 3rd ed., McGraw-Hill, 2003.

[3] Anderson, John D., Fundamentals of Aerodynamics, 5th ed., McGraw-Hill, 2007.

[4] White, Frank M., Fluid Mechanics, 7th ed., McGraw-Hill, 2003.

[5] White, Frank M., Fluid Mechanics, 7th ed., McGraw-Hill, 2003.

[6] Carter, R. T., et al, "Estimating the Drag Coefficients of Meteorites for All Mach Number Regimes," 40th Lunar and Planetary Science Conference, pp. 2059-2060, 2009.

[7] Macrossan, M. N., "Scaling parameters for hypersonic flow: correlation of sphere drag data," Center for Hypersonics, University of Queensland, Brisbane, Australia.

[8] Brown, Louis, A RADAR History of World War II, Institute of Physics Publishing, Bristol, England, 1999 (ISBN 0-7503-0659-9).

[9] Luck, David G., Frequency Modulated RADAR, RCA Labs, McGraw-Hill, 1949.

[10] Headrick, J.M., et al, "A MADRE ICBM Detection: Some Trajectory Parameter Determinations when Employing Ionospheric Refraction," Naval Research Laboratory Report, AD596673, December 1, 1961 .

[11] "Technical Verification Systems, Detection of Reentry Vehicles," Bulletin of the Atomic Scientists, Vol. 41, No 1, p. 39, January, 1985.

[12] West, Adrian, "Detecting Meteors using Radio," http://newburyas.wordpress.com/2009/12/12/detecting-meteors-using-radio/, 7/15/2010.

[13] Barricklow, Sam, "Aurigid Meteor Shower Radio Echoes, September 1, 2007," http://www.k5kj.net/Aurigid_2007.htm, 7/15/2010.

[14] Gamble, Jim, http://elpallskycamera.us, 2010.

[15] P. Spurný, J. Oberst, D. Heinlein (2003). "Photographic observations of Neuschwanstein, a second meteorite from the orbit of the Pribram chondrite". Nature 423 (6936): 151–153.

[16] Oberst, J.; Molau, S.; Heinlein, D.; Gritzner, C.; Schindler, M.; Spurny, P.; Ceplecha, Z.; Rendtel, J.; Betlem, H.. "The "European Fireball Network": Current status and future prospects". Meteoritics & Planetary Science 33 (1): 49, 1998.

[17] http://www.rcktmom.com/njlworks/MeteorTrackingPpr.html

[18] Beatty, Kelly, "Meteorites Found from Asteroid 2008 TC3, http://www.skyandtelescope.com/community/skyblog/newsblog/41873107.html, retrieved 7/10/2010.

[19] Bird, R. B., Steward, W., Lightfoot, E., Transport Phenomenon, John Wiley & Sons, p. 432, 1960.

[20] Kidd, J., and Caldwell, H, USAF, "Defense Support Programs to Support a Changing World," AIAA Space Programs and Technologies Conference, Huntsville, AL, March 24, 1992.

[21] Bayne, Walter J., Air Warfare: An International Encyclopedia,Volume 1, ABC-CLIO, Inc., Santa Barbara, CA, pp. 169 – 172, 2002.

[22] "Lucid Dimensions Spherical Detection Systems (SDS) 3D Passive Infrared (IR)", http://www.defensereview.com/lucid-dimensions-spherical-detection-sds-3d-passive-system, downloaded 7/14/2010.

[23] "Australian laser system to track space junk," http://news.yahoo.com/s/afp/20100720/sc_afp/technologyaustraliasciencespacelaser_2010, 7/20/2010.

[24] Roberto, Rubio, "LIDAR Detection of Subvisible Reentry Vehicle Erosive Atmospheric Material," Army Electronics Command, Fort Monmouth, New Jersey, DTIC Number ADA041085, March, 1977.

[25] Britt, Robert Roy, "Listening for Nukes: A Meteor Detection Project," http://www.space.com/scienceastronomy/solarsystem/nuke_meteor_010524.html, May 24, 2001.

[26] Bedard, A. J., "Infrasonic and Near Infrasonic Atmospheric Sounding and Imaging," U.S. Department of Commerce, http://www.esrl.noaa.gov/psd/programs/infrasound/infrasound.html, 7/15/2010.

[27] Cates, Joseph E., and Sturtevant, Bradford, "Seismic detection of sonic booms," Journal of the Acoustic Society of America, vol. 111, no 1, part 2, pp. 614 – 628, January, 2002.

[28] Koutchmy, S. and Nitshelm, C., "Optical Detection of Space Debris using a Large Achromatic Coronograph," Astrophysics and Space Science, vol. 143, pp. 45-49, 1988.

[29] Garnet, M., and Altman, A., "Identification of Any Aircraft by Its Unique Turbulent Wake Signature," AIAA, Journal of Aircraft, vol. 46, no 1, pp. 263-268, 2009.

[30] Zeiberg, S. and Bleich, G., "Finite-Difference Calculation of Hypersonic Wakes," AIAA Journal, vol 2, no 8, pp. 1396, 1964.

[31] Golovitchev, V. I., and Hansson, J., "Some Trends in Improving Hypersonic Vehicles' Aerodynamics and Propulsion (Fundamentals of AJAX Project)," XIV ISABE Conference, September 5-10, 1999, Florence Italy.

[32] Stepanov, M., "Study of Thermochemical Nonequilibrium in Hypersonic Far Wakes in the Atmosphere," Fluid Dynamics, vol. 37, no 1, pp. 138-146, 2002.